Nano Energy (2015) 12, 419–436

Available online at www.sciencedirect.com

ScienceDirect

journal homepage: www.elsevier.com/locate/nanoenergy

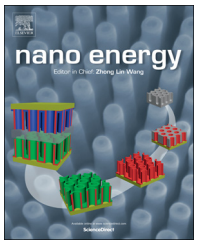

REVIEW

Graphene-based transparent conductive electrodes for GaN-based light emitting diodes: Challenges and countermeasures

Liancheng Wang[a,b], Wei Liu[a], Yiyun Zhang[b,c], Zi-Hui Zhang[a], Swee Tiam Tan[a], Xiaoyan Yi[b], Guohong Wang[b,*], Xiaowei Sun[a,*], Hongwei Zhu[d,*], Hilmi Volkan Demir[a,*]

[a]*Luminous! Centre of Excellence for Semiconductor Lighting and Displays, School of Electrical and Electronic Engineering, Nanyang Technological University, 639798 Singapore, Singapore*
[b]*Semiconductor Lighting Technology Research and Development Center, Institute of Semiconductors, Chinese Academy of Sciences, Beijing 100083, China*
[c]*Department of Electrical and Electronic Engineering, the University of Hong Kong, Hong Kong, China*
[d]*School of Materials Science and Engineering, Center for Nano and Micro Mechanics (CNMM), Tsinghua University, Beijing 100084, China*

Received 30 September 2014; received in revised form 22 December 2014; accepted 24 December 2014
Available online 6 January 2015

KEYWORDS
Graphene;
Light emitting diodes;
Transparent conductive electrodes;
Gallium nitride;
Chemical vapor deposition

Abstract
Graphene, with attractive electrical, optical, mechanical and thermal properties, is considered to be an ideal candidate for transparent conductive electrodes (TCEs) in many optoelectronic devices, including III-nitride based devices. However, high contact resistivity (ρ_c) between graphene and GaN (especially p-GaN) has become a major challenge for graphene TCEs utilization in GaN-based light-emitting diodes (LEDs). Here, we analyzed the graphene/GaN contact junction in detail and reviewed the current research progress for reducing ρ_c in graphene TCEs on GaN LEDs, including interface engineering, chemical doping and tunnel junction design. We also analyzed the current diffusion length for a single layer graphene (SLG) and multiple layer graphene (MLG) TCEs. Finally, to improve the fabrication process compatibility and simplicity with paramount reproduction, a method of directly growing graphene films on GaN by chemical vapor deposition (CVD) is proposed. We also give a short analysis on the reliability of graphene TCEs for GaN-based LEDs. It is believed that this is the ultimate solution for graphene TCEs application for GaN-based LEDs and others in general for other opto- and electrical devices.

*Corresponding author.
E-mail addresses: ghwang@semi.ac.cn (G. Wang), EXWSun@ntu.edu.sg (X. Sun), hongweizhu@tsinghua.edu.cn (H. Zhu), volkan@stanfordalumni.org (H. Volkan Demir).

http://dx.doi.org/10.1016/j.nanoen.2014.12.035

Contents

Introduction

Thanks to their high efficiency, tiny volume, environmental friendliness and long lifespan, GaN-based light-emitting diodes (LEDs) have recently been investigated extensively [1–3]. LEDs find versatile use in general lighting and illumination, information displays, sensors and visible communications. The state of the art conventional lateral LEDs (L-LEDs) are commonly epitaxially grown on insulating sapphire substrates, typically consisting of u-GaN (~3 μm), n-GaN (~3–4 μm), InGaN (~2 nm)/GaN (~8–12 nm) multiple quantum wells (MQWs), and p-GaN layer (~100–200 nm) sequentially. After mesa photolithography and dry etching down to the n-GaN layer, cathode and anode metal contacts will be deposited onto the n-GaN and the p-GaN layers, respectively, from which electrons and holes are injected and recombined within the MQWs. However, restricted by the poor conductance of the p-GaN ($p \sim 10^{17}$ /cm^3), transparent conductive electrodes (TCEs) with both high optical transmittance and excellent conductance are indispensable to spread the injection current away from the metal pads and avoid additional optical absorption to improve the light extraction as much as possible [4].

For vertical LEDs (V-LEDs) [5], fabricated through sapphire removal and new metal standing substrate electroplating, the injection current also tends to crowd under the n-type metal electrodes, especially under high injection current density, leading to a serious decline in luminous efficiency [6]. Excellent TCEs are also necessary for achieving high-performance V-LEDs [7]. Conventional indium tin oxides (ITO) TCEs are widely used in touch sensors, flat panel displays, solar cells and GaN-based LEDs. With great advantages as TCEs, ITO has a low sheet resistance of less than 100 Ω, high optical transparency of ~90%, and unlimited scalability. However, ITO is also criticized for its high cost, poor transparency in the near ultraviolet and ultraviolet ranges, instability in the presence of acids or alkalis, and susceptibility to ion diffusion into the substrate. Moreover, for some flexible devices, ITO is fragile and thus easily cracks during twisting and folding, resulting in the failure of the devices. Moreover, ITO cannot withstand the high temperature procedures, which also limits its application to some extent. Due to these limitations, other novel TCEs are extensively investigated. Graphene, a two-dimensional (2D) material, emerges as an ideal candidate with great potential to replace traditional TCEs and has received great research interest in recent years [8–12]. The outstanding electrical (with reported electron mobility values (μ_n) in excess of 15,000 cm^2 V^{-1} s), optical (with 97.7% transmittance for SLG and absorption saturation), thermal (with near-room temperature thermal conductivity between $(4.84 \pm 0.44) \times 10^3$ and $(5.30 \pm 0.48) \times 10^3$ W m^{-1} K^{-1}), mechanical and chemical properties [12] of graphene make it quite attractive and ideal for application as TCEs.

In this article, we first have a brief introduction about the electronic and optical properties of graphene. In the following we reviewed and summarized research progress, current related approaches and developments from both our and other groups for graphene TCEs utilized in

GaN-based LEDs. More details will be introduced on our tunnel junction design to reduce the ρ_c between p-GaN and graphene. For simplifying the fabrication process and improving the adhesion of graphene, we also provide a review on graphene local growth on GaN so far. Through our analysis, we think this is the ultimate solution to overcome the fabrication compatibility and adhesion problem, which paves the way for the ultimate application of graphene TCEs on GaN-based LEDs.

Electronic and optical properties of graphene

Graphene is a single planar sheet of sp^2 bonded hybrid carbon atoms with s, p_x and p_y atomic orbitals on each carbon atom forming three strong σ bonds with other neighboring atoms. The remaining p_z orbital of each carbon atom produces a filled band of π orbital (valence band) and an empty band of π^* orbital (conduction band) [13,14]. The electronic wave-functions from different atoms overlap, except for the p_z (π) orbital and the others, p_x and p_y atomic orbitals - the overlap is strictly zero due to symmetry. Consequently, the p_z electrons formed π orbitals can be treated independently and with this π-band approximation, the dispersion relations $E(k_x, k_y)$ can be easily obtained [15]:

$$E^{\pm}(k_x,k_y)=\pm\gamma_0\sqrt{1+4\cos\frac{\sqrt{3}k_xa}{2}\cos\frac{k_ya}{2}+4\cos^2\frac{k_ya}{2}} \tag{1.1}$$

where $a=\sqrt{3}a_{cc}$, a_{cc}=1.44 Å being the carbon-carbon lattice distance and γ_0 is the transfer integral between the first-neighbor π orbitals. The $k=(k_x, k_y)$ represents the ensemble of the available electronic momenta in the first Brillouin zone. The valence band and conduction band touch at the six two-dimensional hexagonal Brillouin corners (Dirac points, K), making graphene a semi-metal or zero-gap semiconductor. Expanding equation (1.1) for low energies near the K points yields the following linear dispersion relationship:

$$E(k)=\pm\hbar V_F|k| \tag{1.2}$$

where $k=K'-K$, as measured from the Dirac points and v_F ($\sim10^6$ m/s) is the electron group velocity. Figure 1(a) shows the band structure of graphene (left) and the zoom-in of the energy bands close to one of the Dirac points (right) [14]. The semimetal behavior and massless Dirac fermions characteristics of graphene revealed by the band structure, shown in Figure 1(a), theoretically ensure its superior electrical, optical and thermal properties, such as high carrier mobility, almost wavelength-independent and saturable optical absorption, etc. Figure 1(b1) shows the transmittances of SLG ($\sim$97.7%) and bilayer graphene ($\sim$95.4%) [16]. Geim et al. [16] found that the opacity of an SLG is defined solely by a series of fundamental constants: fine structure constant $\alpha=e^2/\hbar c\approx 1/137$ (where c is the speed of light), and physically describes coupling between light and relativistic electrons:

$$T_{SLG}=(1+0.5\pi\alpha)^{-2}\approx1-\pi\alpha=97.7\% \tag{1.3}$$

Additionally, graphene only reflects <0.1% of the incident light in the visible region, and this reflectance reaches only to $\sim$2% for ten layers. The transmittance of MLG is linearly proportional to the layer number, n:

$$T_{MLG}=1-nA_{SLG}=1-2.3\%\cdot n \tag{1.4}$$

where A_{SLG} represents the absorption of each layer, with $A_{SLG}=1-T$=1-97.7%=2.3% over the visible spectrum. MLG can be optically equivalent to the simple stack of SLG, with little perturbation of each adjacent layer. Moreover, graphene shows a quite flat absorption spectrum over a very wide region (400-2500 nm) and saturation absorption characteristics when the input optical intensity is above a threshold value (Figure 1(b2) [16]). Inset of Figure 1(b2) shows the transmittances of white light as a function of the number of graphene layers [16].

Current approaches for graphene TCEs utilization in LEDs

The state-of-the-art of graphene TCEs

Various approaches have been explored to obtain graphene-based TCEs, including: micromechanical cleavage[17], CVD growth on metal substrate [18-22], chemical reduction of graphene oxide [23,24], spraying [25], dip [26], spin coating [27], vacuum filtration [28] and roll-to-roll processing [29]. Considerable progress has been made since the first attempt to produce graphene-oxide-based TCEs. Gilje et al. [25] decreased R_s from 40 GΩ/sq to 4 MΩ/sq following reduction with dimethylhydrazine. Graphitization, hydrazine exposure and low-temperature annealing, or high-temperature vacuum annealing further decreased R_s down to 800 Ω/sq for T=82%. Novoselov et al. [17] reported graphene TCEs prepared by micromechanical cleavage with $T\approx98\%$ and R_s=400 Ω/sq using a layer of polyvinyl alcohol to induce n-type doping. TCEs have been produced using the ultra-large graphene oxide sheets that are deposited layer-by-layer on a substrate using the Langmuir Blodgett (LB) assembly technique developed by Jang-Kyo Kim's group [30].

After thermal reduction and chemical doping, R_s of 500 Ω/sq and T of 90% have been obtained. By intercalating micromechanical cleavage MLG with $FeCl_3$, R_s of 8.8 Ω/sq and T of 84% have been obtained by Craciun group [31]. Bae et al. [29] reported the roll-to-roll production and wet-chemical doping of predominant monolayer 30-in. graphene films grown by CVD onto flexible Cu substrates, reaching a low R_s of 125 Ω/sq and T of 97.4%. Figure 1(c) is a summary for graphene TCEs R_s and T reported from different groups. It shows that graphene TCEs derived from the CVD method (especially on Cu), combined with doping, could outperform the conventional ITO TCEs. Moreover, as is known, T is dominated by the layer number (n) of graphene, with $T=1-n\pi\alpha$, where $\pi\alpha\approx2.3\%$ is the absorption for a single layer. It seems the "trade-off" rule that the lower sheet resistance will naturally come with the higher opacity (corresponding to larger n) also works for graphene TCEs. However, for the-state-of-art of CVD grown and transferred graphene TCEs, defects (such as dislocations, steps and grain boundaries) formed during the CVD process, and disruptions (such as wrinkles, cracks and edges) formed during the transfer process, can scatter the charge carriers, leading to the degradation of the transport properties of graphene and lower electrical conductivity [32].

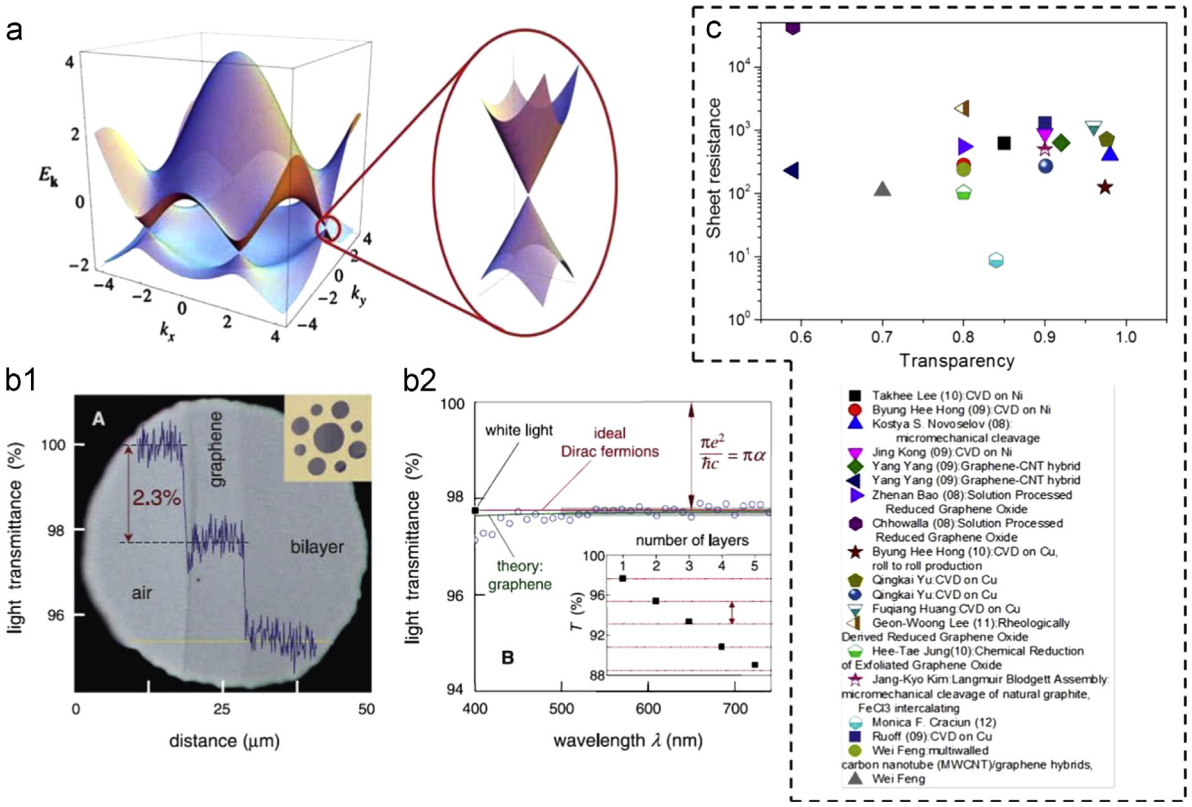

Figure 1 (a) Shows the band structure of graphene (left) and zoom-in of the energy bands close to one of the Dirac points (right) [14]; (b1) shows the transmittances of single-layer (SLG) (~97.7%) and bilayer graphene (~95.4%) [16]; (b2) shows the transmittance of graphene versus light wavelength. Copyright from AAAS. [16]. Inset of (b2) shows the transmittances of white light as a function of the number of graphene layers [16]; (c) summarizes the sheet resistance and optical transmission for graphene TCEs reported from different groups.

By making efforts to bring down the defects during growth and transfer, or by healing the defects through metal nanowires, graphene conductivity can be further improved while keeping its optical transparency [33] intact. Note that graphene TCEs mentioned and discussed later on in this paper are grown by the CVD method, except where specially clarified.

To function perfectly as TCEs, besides the high T and low R_s as mentioned above, there are several other requirements including strong adhesion and good ohmic contact to the target substrate. When graphene is transferred onto GaN LEDs, we need to guarantee that the electrons can effectively transport from graphene into GaN, which means the electrons can transport across the p-GaN/graphene (L-LEDs) or u-, n-GaN/graphene (V-LEDs) hetero-junction with resistance as low as possible. However, due to the large work function (W_F) mismatch between graphene (~4.8 eV for weak p-doped) and p-GaN (~7.5 eV), u-, n-GaN (~4.0 eV), the high interface contact barrier (Ψ_b) would hinder the movement of carriers (electrons or holes) and increase the R_c, leading to the higher operating voltage (V_F) of LEDs ultimately. And this large ρ_c value at GaN/graphene, especially for p-GaN/graphene junction, indeed has become the most challenging obstacle for graphene TCEs application on GaN-based LEDs. Furthermore, considering the compatibility of graphene in LEDs' fabrication processes, the poor adhesion between graphene and GaN poses another unavoidable and critical problem, and severely affects the LED reliability.

Metal-graphene contact

Fig. 2(a1) and (b1) shows the schematic drawings of L-LEDs and V-LEDs incorporating graphene TCEs. Fig. 2(a2) and (b2) shows the corresponding emission micrograph images of L-LEDs and V-LEDs. Fabricating LED devices with graphene TCEs will essentially involve making metals contacts. Therefore, before introducing graphene TCEs contact with GaN in GaN LEDs, it is necessary and prudent to better understand the contact properties between metal and graphene.

Graphene-metal contacts category

Owing to the vanishing density of states (DOS) approaching the Dirac points, even a small amount of transfer of electrons will shift the Fermi level (E_F) significantly ($\Delta E_F = W_M - W_G = 0.47$ eV when 0.01 electrons transferred). Intuitively one could assume that an electron is transferred into (withdrawn from) graphene when $W_G > W_M$ ($W_G < W_M$), and $\Delta E_F = 0$ when $W_G = W_M$. However, Giovannetti et al. [34] found that the crossover point lies at $W_M - W_G = 0.9$ eV. Through further first-principle calculations at the level of density function theory (DFT), they stated that metals can be divided into two classes. Ran [35] further states that the projected DOS of the metal's d-orbital dominates the formation of physical/chemical contact. Chan et al. [36] state that contacts between group I-III metal atoms and graphene are ionic, while the transition metals make covalent bonds with graphene. Therefore, graphene-

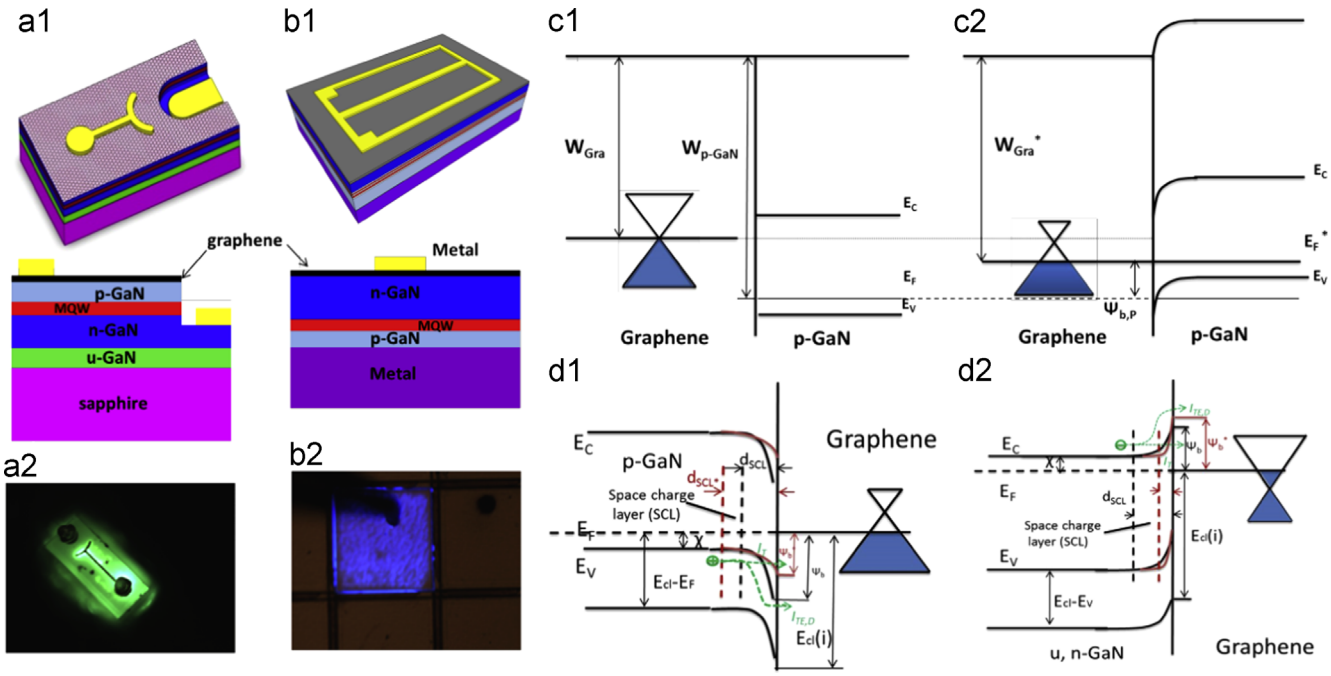

Figure 2 (a1) and (b1) show the schematic drawing of lateral and vertical LED devices with graphene TCEs; (c1) and (c2) show the sketch band diagram of graphene/p-GaN junction before and after alignment; (d1) and (d2) show the schematic band structures and carriers transportation when graphene contacts with p-GaN and n-GaN.

Table 1 (a) Two categories of metal contact with graphene; (b) summary of the obtained Ψ_b by different groups and different methods.

(a)

Strong contact metal	Ni, Co, Pd, Ti, Cr
Weak contact metal	Al, Ag, Cu, Au, Pt, Ir, Ga

(b)

	Theoretically predicted value (Ψ_b^T)	S. Tongay group	Haijian Zhong group	Our group	
				I-V fitting (Ψ_b^F)	XPS (Ψ_b^X)
Graphene/n-GaN	0.7	0.73	0.33±0.01	0.36±0.01	0.57
Graphene/p-GaN	2.7	NA	0.36±0.01	0.49±0.02	2.08
Graphene/n-Si	0.75	0.86	NA	0.78	NA
Graphene/n-GaAs	0.7	0.79	NA		

metal contacts can be divided into two classes (Table1(a)): chemisorbed graphene-metal contacts such as graphene-Ti, Co, Ni, Pd, with an equilibrium separation $d_{eq}\sim 2$ Å, in which the graphene bands are strongly perturbed and will acquire a mixed graphene-metal character; and physical absorbed graphene-metal contacts such as graphene-Al, Cu, Ag, Au, Pt, with an equilibrium separation $d_{eq}>3.2$ Å, in which graphene retains its unique bands characteristics with metal physically contacted.

Graphene-metal contacts resistivity

On the other hand, reported values of metal-graphene ρ_c vary and appear to depend on the metal used, fabrication procedure, gate bias, measurement conditions and even metal microstructure: a gate-dependent ρ_c of 500 Ω μm of Ni-graphene at 300 K, 700±500 Ω μm for Ti-graphene [37], 185±20 Ω μm at 300 K and 120±20 μm at 6 K [38] and $\sim 5\times 10^{-6}$ Ω cm^2 for Ni-graphene using the cross-bridge Kelvin structure [39]. Xia [40] used Landauer's approach [$G=(4e^2/h)TM$, where M is the number of the conduction mode in graphene, T is the transmission probability] to understand metal-graphene ρ_c, and mechanisms such as charge transfer [34,41,42], gate dependence of the Dirac point energy, broadening of DOS (as electron-hole puddle formation) and carriers tunnel probability as a function of the interfacial potential barrier width, shape and height are considered. Ji [43] further considered the Fermi velocity difference of graphene under and away from metal. In GaN LEDs, metal systems usually contain Ni/Au, Cr/Pt/Au, Al/Ti/Au or Ti/Al/Ti/Au. Metal-graphene ρ_c are in the range of 10^{-5}-10^{-6} Ω cm^2, according to the reports mentioned above and our group [37-39,66]. The corresponding voltage

drop can be negligible, which is calculated to be ~0.01 V at 1 A forward operating current for a $320 \times 320\ \mu m^2$ contact ($\Delta V = IR = I\rho_c/S = 1\ A \times 10^{-5}\ \Omega\ cm^2/10^{-3}\ cm^2$). The interfacial metals Ni, Ti and Al belong to the chemical and physical contact class, respectively, according to Ref. 34.

Attributed to the fact that Cr has a half-filled 3d-electron shell ([Cr]$3d^5 4s^1$), the most stable configuration (along with full filling $3d^{10}$), Cr/graphene should be the physical contact type. Generally, graphene TCEs cover the whole chip and the area ratio between metal and graphene is ~10%, as can be seen from Fig. 2(a1) and (b1). Nevertheless, this metal-graphene contact can be still evaluated using Fengnian Xia's modified Landauer model [40]. According to the above discussion, the chemisorbed metal would distort the band structure of graphene and the physical absorbed metal has negligible influence on that. This metal-induced variation on graphene would thus have an effect on graphene/GaN contact properties. However, in all the published articles related to graphene TCEs in GaN LEDs, the influences of metal on graphene-GaN contact are neglected. Understanding the interplay of metal-graphene-GaN is inspiring and of great significance. Furthermore, the principle for metal/graphene contact is actually similar to that of graphene CVD growth on metal; hence, understanding this can also help reveal the mechanism of CVD graphene growth on different metal substrates. This is beneficial for understanding graphene local growth on GaN substrate, which will be discussed later in this article.

GaN/graphene contact

It is important to understand the graphene/GaN interface physics and transport mechanism for carriers transporting across it. The Tongay group [44,45], the Zhong group [46] and our group [47] have obtained the Schottky barrier height (Ψ_b) by fitting graphene-GaN *I-V* curve using the thermionic emission theory, i.e., the Richardson equation:

$$I = AA^*T^2 \exp(-q\psi_b/kT)\left[\exp\left[\frac{q(V-IR_s)}{nkT}\right]-1\right] \tag{2.1}$$

where A is the contact area, A^* is the Richardson constant (26.4 A cm^{-2} K^{-2} for n-GaN and 96.1 A cm^{-2} K^{-2} for p-GaN), R_s is the series resistance and n is the ideality factor. Taking Ψ_b, R_s and n as fitting parameters, Ψ_{bp} and Ψ_{bn} can be statistically determined. Table 1(b) summarizes the obtained Ψ_b by different groups as mentioned above. Ψ_b for graphene/Si, GaAs junctions were also listed as reference. Superscripts *T*, *F* and *X* for Ψ_b denote theoretically calculated, *I-V* fitted and XPS test results, respectively. Ψ_b^T was simply estimated based on the difference between W_F(G) and χ.

Zhong [46] and our group's results [47] unambiguously show that Ψ_b^F is rather lower than Ψ_b^T. However, Tongay's [44] results show comparable value between $\Psi_{b,n}^T$ and $\Psi_{b,n}^F$, yet they did not provide $\Psi_{b,p}^F$ results, making comparison incomplete. Like the graphene/metal contact, electrons transferred into (out of) graphene, raise up (brings down) the E_F of graphene when it contacts with n-GaN (p-GaN), leading to a lower $\Psi_{b,n}^F$ ($\Psi_{b,p}^F$). Zhong [46] claimed this self-adaptive shift of E_F in graphene to be the dominant reason accounting for the differentiation between Ψ_b^T and Ψ_b^F. XPS tests have been further carried out by our group [47] and the corresponding Ψ_b^X values are also listed in Table 1(b). Ψ_b^X falls between Ψ_b^T and Ψ_b^F, especially $\Psi_{b,p}^X$ (2.08 eV) is significantly higher than $\Psi_{b,p}^F$ (0.49 eV). We believe Ψ_b^X most closely approaches the real Ψ_b.

Understanding the discrepancy between Ψ_b^T and Ψ_b^X

First, we assume the aforementioned self-adaptive-E_F-shift in graphene to be the sole reason contributing to the discrepancy between Ψ_b^T and Ψ_b^X. figure(c1) and (c2) shows sketches of the graphene/p-GaN junction before and after alignment, with $\Delta W_{Gra} = W_{Gra}^* - W_{Gra}$ equal to the variation of graphene work function due to self-adaptive effect. Here, electrons transferred out of graphene lead to $E_{F,G}$ being reduced,. We denote $N_{transferred}$, $\Delta E_{F,G}$, to be the number of the transferred electrons per unit area, shifted E_F,

$$\Delta E_{F,G} = -\mathrm{sign}(N_{transfered})\sqrt{2N_{transfered}/(q^3 D_0)} \tag{2.2}$$

$$N_{transfered} = \sqrt{2q\xi_r\xi_0 N^* V_{D,p\_GaN}} \tag{2.3}$$

$$eV_{D,p\_GaN} + \chi = \varphi_{b,p};\ \ \chi = e(E_{F,p\_GaN} - E_{V,p\_GaN}) = k_b T \ln(N_v/p) \tag{2.4}$$

where Eq. (2.2) is obtained by integrating the linear DOS, $D_0 = 0.09\ eV^2$ per unit cell for E within 1 eV of the conical points. It is well known that the Schottky barrier values are well described using either Bardeen or Schottky limits. Many experiments have demonstrated that the ionic wide gap semiconductors SiC and GaN are managed by the Schottky-Mott (S-M) limit [48-50]. Hence, the graphene/GaN interfacial states are neglected in our model, in contrast with Haijian Zhong's model. $\Delta E_{F,G}$ is first assumed to be equal to 0.62 eV ($\Psi_b^T - \Psi_b^X$=2.7-2.08 eV). $V_{D,\ p\text{-}GaN}$ can be derived from Eqs. (2.2) and (2.3), finally the $\Psi_{b,p}$ value can be obtained from Eq. (2.4). Finally, the $N_{transferred}$ value obtained from Eq. (2.3) is $2.394 \times 10^{13}\ cm^{-2}$ and $\Psi_{b,p}$ was found to be ~0.36 eV (assuming $E_F - E_v$=0.13 eV), which is significantly lower than $\Psi_{b,p}^X$ (2.08 eV).

It is noteworthy that the above-mentioned calculations are based on a simple self-adaptive model. There are several possible reasons accounting for the discrepancy between $\Psi_{b,p}^X$ and $\Psi_{b,p}^T$. First, $E_{F,G}$ may lie far away from (typically below) the Dirac point before graphene contacts with GaN. The deviation can be attributed to hole doping of the graphene during the Fe(III)NO_3 etching-transfer process [51,52]. Therefore, instead of Eqs. (2.2) and (2.3), $N_{transferred}$ should be modified as follows:

$$\Delta E_{F,G} = \left|E_{F,G} - E_{F,G}^0\right| \tag{2.5}$$

$$E_{F,G}^0 = -\hbar\left|v_F\right|k_{F0} = -\hbar\left|v_F\right|\sqrt{\pi N_0} \tag{2.6}$$

$$E_{F,G} = -\hbar\left|v_F\right|k_F = -\hbar\left|v_F\right|\sqrt{\pi(N_0 + N_{transfered})} \tag{2.7}$$

where $\hbar = 6.5 \times 10^{-16}$ eVs, v_F is the Fermi velocity of $\sim 1.1 \times 10^8$ cm/s and $E_{F,G0}$ is calculated to be 0.287 eV below the Dirac point when $N_0 = 5 \times 10^{12}\ /cm^2$, a shift associated with the aforementioned p-doping during processing. Again it is assumed that $\Delta E_{F,G}$ is 0.62 eV. Then accordingly, $N_{transferred}$ can be calculated to be $\sim 4.5 \times 10^{12}\ /cm^2$. By substituting

$N_{transferred}$ back into Eqs. (2.3) and (2.4), the $\Psi_{b,p}$ value can be calculated to be ~1.18 eV. It is still much lower than $\Psi^X_{b,p}$. Except for the $E_{F,G}$ divergence, the discrepancy between the calculated $\Psi_{b,p}$ and $\Psi^X_{b,p}$ values might also be attributed to: (1) the formation of an interface dipole at the graphene/GaN interface, serving as a plane capacitor (within the bond polarization theory) [53-55].

Gong et al. [56] have proposed the metal/graphene/metal sandwich geometry to strengthen the interface interaction. He suggests that interface charge repulsion occurs, resulting in charge redistribution away from the interface into both metal slabs and within the graphene basal plane. The electron accumulation graphene plane formed allows the antiparallel dipole throughout the interface to interact constructively in the parallel alignment due to the alternative reservoirs of the opposite charges. Considering the metal/graphene/GaN sandwich structure (even graphene is partly covered by metal), a more complex charge redistribution phenomenon may occur; (2) according to Giovannetti's work [34], the top metal Cr may interrupt the intrinsic π band structure of graphene by internal chemisorption. All these will have an impact on the equilibrium band alignment, and thus Ψ_b.

Understanding the discrepancy between Ψ^F_b and Ψ^X_b

Let us recall the *I-V* test and compare Ψ^F_b and Ψ^X_b. Generally, there are several mechanisms accounting for the carriers transporting across the GaN/graphene interface: thermal emission-diffusion and tunnel [57,58], with its corresponding current denoted as $I_{TE,D}$ and I_T, respectively. figure(d1) and (d2) show the schematic band structures and carriers transportation when graphene contacts with p-GaN and n-GaN. We attribute the discrepancy between Ψ^F_b and Ψ^X_b to the carrier tunnel transport component, whose flow path is in parallel with the thermal emission-diffusion component ($I_{TE,D}$) and was totally neglected in Eq. (2.1). So the obtained I is actually the sum of I_T and $I_{TE,D}$, and Ψ^F_b obtained from the *I-V* fitting is actually a counterfeit barrier height.

Tunnel probability is related to the density of defects and dislocations located in the interface or space charge zone, acting as the multiple tunnel paths for carrier transport [59,60]. Owing to the lattice mismatch of epitaxial GaN on sapphire (~16%), high-density dislocations (~10^8 /cm^2) make I_T even become dominant on GaN-based contact. Referring to Tongay' work [45], we noticed that it is commercial n-type GaN they used, which usually demonstrate a lower dislocation density than that of GaN epitaxial layer on sapphire. This of course will bring down I_T and the obtained Ψ^F_b value approaches our Ψ^X_b value. Refer to graphene/n-Si Schottky solar cells, which have been successfully demonstrated by our group [12,61,62]. The Schottky barrier height has been derived to be ~0.78 eV from *I-V* fitting, in agreement with the theoretically predicted Ψ^T_b ($=W_G-\chi=4.-4.05$ eV$=0.75$ eV). Low I_T and high $I_{TE,D}$ is one of the prerequisites for solar cells working. In the purest crystalline Si (with the lowest defect density) junction the carrier tunnel is inhibited, which is just opposite to the case of graphene/GaN contact where I_T is dominant. Temperature-dependent *I-V* characteristics from our group [47] and the Chandramohan group [63] further confirm the existence of the I_T component in graphene/GaN contact.

Next we turn our attention to the effect of bias on $W_{F,G}$ [64], and thus on Ψ^F_b. Unlike conventional metals, graphene's work function $W_{F,G}$ is a function of bias and the SBH value and does not remain constant. For graphene/n-GaN junction, when forward (reverse) bias is applied the graphene will be positively (negatively) charged. Correspondingly $E_{F,G}$ will decrease (increase), $W_{F,G}$ will increase (decrease), causing Ψ_b to increase (decrease). The fixed SBH assumption during the *I-V* fitting no longer holds. This is similar to the aforementioned self-adaptive effect. Typically the reverse biased voltage is much larger compared with the forward bias, usually leading to significant reduction in Ψ_b. Tongay et al. [44] have observed the non-saturating reverse current in graphene–semiconductor junctions, but not in graphite and metal-based Schottky junctions, due to the fixed Fermi level of the latter.

Experimentally derived graphene/GaN contact resistivity

The p- and n-GaN/graphene junctions are both reverse biased when LEDs are operated at forward bias. It is meaningful to know the specific R_c values of contact between graphene and different GaN (n-GaN, u-GaN, p-GaN), as for different LED structures, graphene films were deposited on the GaN surfaces with different doping types, concentrations and polarities. We have used a conventional circular transmission line method (CTLM) to obtain ρ_c [65,66]. Although the charge transfer doping effect and other possible band variations in metal/graphene/GaN system are inevitable and there is complexity inferred from our discussion in metal/graphene contact, we still can first overlook these factors in ρ_c calculation. After dissolving the metal substrate and transferring the CVD-grown graphene onto the GaN surface, metal Cr/Pt/Au with a CTLM pattern was deposited. The CTLM patterns consist of 100 μm [2] ohmic pads with gap spacings of 10, 20, 30, 40, 50 and 60 μm. By reasonable and rational approximation, ρ_c values of graphene/Cr, p-GaN, u-GaN, n-GaN, N-polar u-GaN and N-polar n-GaN are fitted and calculated to be $\sim 0.9\times10^{-5}$, $\sim 4.3\times10^{-1}$, $\sim 3\times10^{-2}$, $\sim 1.1\times10^{-5}$, $\sim 2.4\times10^{-2}$ and $\sim 0.9\times10^{-6}\ \Omega\,\mathrm{cm}^2$, respectively. It can be concluded that, in case of a given graphene, ρ_c values of graphene/GaN contacts are mainly determined by W_F gap and carrier concentration of GaN; that is to say, a lower W_F mismatch and a higher carrier concentration will lead to lower ρ_c. Various defects and impurities could be generated during laser lift off (LLO) and inductively coupled plasma (ICP) processes in N-polar GaN fabrication process [67]; we believe this could bring down the ρ_c values for graphene/N-polar GaN contact. Huang et al. [68] found that the MQWs-covered graphene can screen of the polarization field in the c-plane GaN-based quantum well. This would have a negligible effect on graphene/GaN contact, however.

Graphene on conventional lateral LEDs

Jo et al.[69] first demonstrated MLG-TCEs in blue LEDs. The MLG-TCEs LED shows V_F (~5.6 V@20 mA) and 37% lower light output power (LOP), compared with ITO TCEs LED (~3.8 V@20 mA). Seo et al. [70] demonstrated a graphene TCEs LED exhibits ~25% improved LOP and increased V_F to 5.87 V from 3.4 V compared to the ITO TCEs LED,

respectively. Kim [71-73] first attempted incorporating graphene TCEs in ultra-violet (UV) LEDs, which exhibited significantly high V_F (26.5 V@1 mA). Even though benefiting from the aforementioned self-adaptive, tunnel and electrical doping effects, R_c, the value of graphene/p-GaN contacts is still too large. Taking ρ_c to be $4.3 \times 10^{-1}\ \Omega\ cm^2$ (as calculated above) and the contact area S (almost equal to the chip area) to be $\sim 10^{-2}\ cm^2$, the voltage drop across the graphene/p-GaN junction will be $\sim$0.86 V and $\sim$15 V at 20 mA and 350 mA forward currents, respectively. Here we will summarize the efforts being devoted to ρ_c reduction for graphene TCE applications in conventional lateral LEDs, including approaches such as interface engineering, chemical doping, annealing, etc.

Interface engineering

Through graphene/p-GaN interface engineering to create virtually hybrid graphene, TCEs is one of the most feasible approaches. The design rule is to insert an interlayer sandwiched between graphene and p-GaN, as shown in Figure 3(a). The interlayer should be transparent, conductive and have low ρ_c with both p-GaN and graphene. The choice of interlayer materials includes: Ni [74], NiO_x [63,75], ITO [76,77], ZnO nanorods [78,79], Ag [80-83], Au nanoparticles [84-86], AgNWs (Ag nanowire), etc. Table. 2 lists the reported graphene hybrid structure, features and corresponding chip results. The interlayer generally reduces ρ_c and V_F. However, it often reduces the T as well ($\sim$10-20% loss after interlayer insertion). Normally, the final graphene hybrid TCEs-based blue LEDs' electrical and optical characteristics lie between that of bare graphene and conventional ITO-based blue LEDs. Notably, in the UV region, graphene hybrid TCEs-based LEDs beat that of conventional ITO TCEs due to graphene's wavelength-independent transmission even in the UV region.

Chemical doping

Generally speaking, the principle of chemical doping to improve graphene/p-GaN contact is to introduce foreign electron withdrawing agents onto the surface of graphene which leads to p-type doping and thus increases W_F of graphene [29,87-89], as shown in Figure 3(b1). Bae et al. [29,84-86,90,91] tested various wet doping agents and the results are summarized in Figure 3(b3). They found that $AuCl_3$ in Nithomethane and HNO_3 are among the most efficient doping agents. Researchers from different groups have demonstrated an improvement of electrical and optical characteristics of blue and near UV LEDs with Au-doped graphene TCE-based LEDs, as can be clearly seen in Table. 3. We also used HNO_3 [47,92] evaporations to dope the graphene TCEs and the experimental set-up is shown in Figure 3(b2). The p-(n-)GaN/graphene band diagram

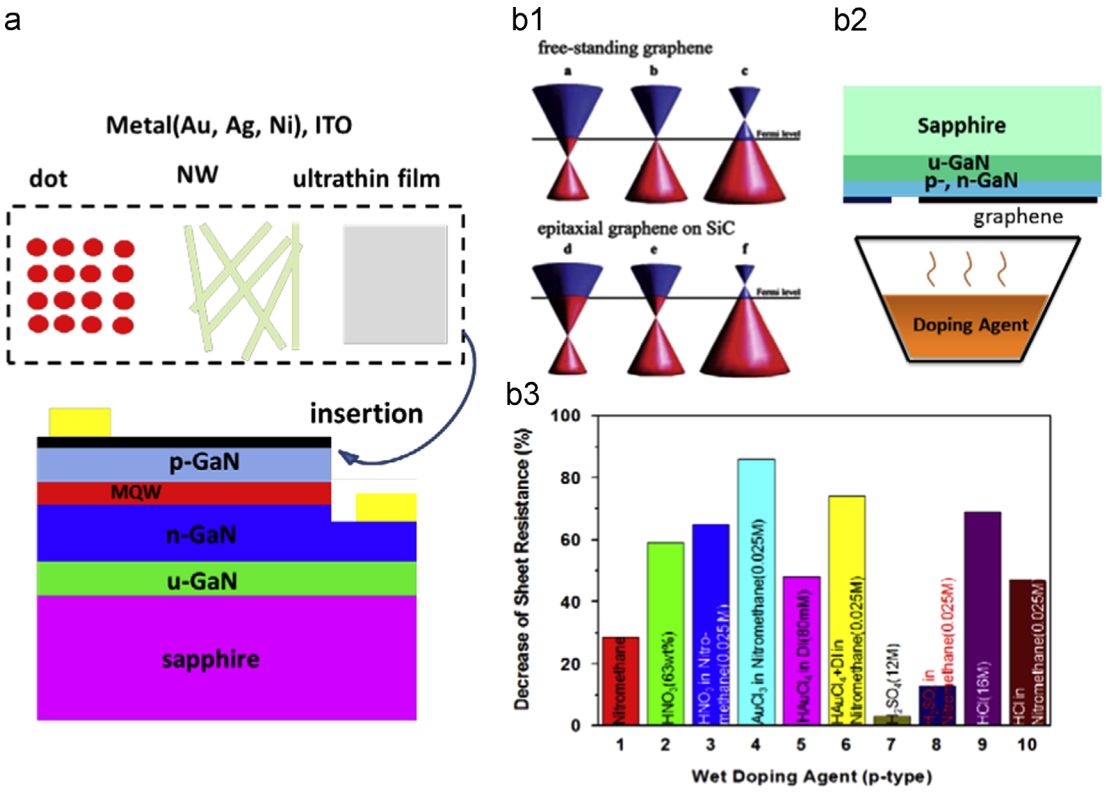

Figure 3 (a) Sketch of the principle of interface engineering approach for graphene TCEs utilization: metal (Au, Ag, Ni) and ITO dot, NW and ultra-thin film are inserted between graphene TCEs and p-GaN; (b1) schematic diagram of the position of the Dirac point and the Fermi level as a function of doping. The upper panel is n-type doped, pristine and p-type doped free-standing graphene (a-c). Copyright from RSC. [87]. The lower panel is n-type doped, pristine and p-type doped graphene grown on silicon carbide (SiC) (d-f); (b2) shows the experimental setup for HNO_3 [47,92] evaporation graphene doping; and (b3) summarized decrease of sheet resistance by using various wet doping agents. Copyright from NPG. [29].

Table 2 The reported interface engineered graphene hybrid structure, feature and its corresponding chip results.

TCEs structure	TCEs feature			Chip feature	ρ_c (Ω cm^2)	Chip characterization
		T	R_s (Ω/sq)			
AgNWs/Gra (with different AgNWs concentration) [83]	0.1 mg/ml	96.7%	801		Gra/p-GaN:1.06;	Gra/AgNWs: 8.4 V, 7.8 V, 6.6 V@20 mA, respectively
	0.5 mg/ml	96%	645	177.8 × 228.6 μm^2	Gra/AgNWs/p-GaN:	Bare Gra: 11.8 V@20 mA
	1.0 mg/ml	92.8%	367	460 nm	1.05×10^{-1}	
AgNWs/Gra [82]	AgNWs/Gra	86.3%	500±100	350 × 350 μm^2	NA	Bare Gra: 10.9 V@20 mA; AgNWs: 6.7 V@20 mA;
	Bare gra	93%	30±3	UV (375 nm)		AgNWs/Gra: 4.48 V@20 mA; 250% EL improvement (AgNWs/Gra compared with bare gra)
ITO dot (7-10 nm)/Gra	Single Gra	96.7%@460nm; (88.2%@320 nm)	800-1000	254 × 254 μm^2	NA	Bare Gra: 6.76 V@20 mA
cold wall rapid CVD growth[77]	Mltilayer Gra	91.7%@460 nm; (81.9%@320 nm)	300-350			ITOdot/Gra: 3.9 V@20 mA Conventional ITO: 3.6 V@20 mA;
NiOx (1 nm)/Gra[75]	T=90%			225 × 175 μm^2	Gra/NiOx/p-GaN: 5.9×10^{-4}	@20 mA: 3.65 V (Gra/NiOx); 6.15 V (bare Gra); 3.2 V(ITO)
NiOx (2 nm)/Gra[63]					Gra/NiOx/p-GaN: 8.8×10^{-1}	@20 mA: 3.16 V(Gra/NiOx); 4.5 V(Bare Gra) Lower output power of Gra/NiOx TCEs
Ni/Ag/Gra/ZnO nanorods79	t~70-80%				0.5	2.5 V@0.01 mA 66% EL increased over bare Gra
ITO dots /Gra[76]	Diameter 150 nm, density 3.8×10^9 cm^2, T=85%@550 nm; $R_s = 2.2 \times 10^3$					@20 mA: 6.4 V(bare Gra); 6.1V(ITO dots); 3.66V (ITO dots/Gra) 1.5 times LOP increases (ITO dots over bare Gra)
ITO dots /Gra (Gra grown by chemical)	T~90%			315 × 315 μm^2		@20 mA: 5.9 V (bare Gra); 4.9 V (Gra on ITO dots); 4.42 V (CCG on ITO dots); 4.35 V (conventional ITO)
				UV LED (~380 nm)		EL increases 150% and 60% for CCG/ITO and graphene ITO over conventional ITO, respectively
(p-GaN)/Gra/Ni (3 nm) [74]	Gra/Ni	75%	690±50			Blue @20 mA: 6.2 V (bare Gra) UV @20 mA; 13.2 V (Gra)
	Gra	90%	1250±50			
	ITO	86%@460 nm	43±5	Blue:460 nm		
		70% @380 nm		UV:380 nm		3.5 V (ITO) 50% decreased EL over ITO 7.1 V (Gra/Ni) 83% EL of ITO

Table 3 Electrical and optical characteristics of blue and near ultra-violet LEDs with Au-doped graphene TCE-based LED.

Graphene doping agent		TCEs feature			Chip results		
		W_F (eV)	T	R_s	I-V	EL	Peak wavelength
$AuCl_3$ [90]	0 mM	4.42	89%	1000 ± 698	4.73 V@0.4 mA	1	460 nm
	5 mM	4.77	85%	203 ± 37	3.94 V@0.4 mA	1.938	
	20 mM	5.12	78%	105 ± 7	3.86 V@0.4 mA	1.287	
Au nano particle [82]	Bare Gra	NA	88%	1000 ± 100	7.8 V@20 mA	1	415 nm
	Au-Gra	NA	88%	18 ± 2	6.8 V@20 mA	1.34	

variation after HNO_3 treatment is also shown in figure(d1) and (d2) (red line), respectively. Decreased Ψ_b or narrowed space-charge layer will initiate a higher percentage of I_T, causing a reduction in ρ_c. Both L-LEDs and V-LEDs (3.17 V@350 mA, 3.64 V@1000 mA) show decreases in V_F and ~19% enhancement in LOP. Note that doping will decrease the carrier mobility of graphene and the corresponding effect on its conductivity should be checked.

Current diffusion length (L_s) analysis for graphene TCEs

Taking $R_s \sim 1000\ \Omega/\text{sq}$ and $\rho_c = 1\ \Omega\,\text{cm}^2$, current diffusion length L_s in SLG TCEs can be roughly calculated to be $L_s \approx \sqrt{\rho_c/R_l} = \sqrt{1\ \Omega\,\text{cm}^2/100\ \Omega} = 316\ \mu m$. For a typical interdigital patterned metal contact in a 1 mm × 1 mm device, L_s is much larger than the neighbored metal space width (~250 μm), indicating that even the R_s of the state-of-the-art SLG is huge, and SLG can still efficiently spread the current to achieve uniform distribution thanks to the "current blocking effect" of the relatively large "vertical resistance" ρ_c. However, the relatively larger ρ_c would add to the series resistance ($R = R_c/S = 1\ \Omega\,\text{cm}^2/0.01\ \text{cm}^2 = 100\ \Omega$) and ultimately increase the device V_F ($\Delta V = RI = 100\ \Omega \times 0.35\ \text{A} = 35\ \text{V}$).

$$R_s = \frac{\rho}{t} = \frac{1}{nq\mu_n t} \propto \frac{1}{N^*},\quad \rho_c \propto P \propto \exp\left[-\frac{2eV_D}{e\hbar(N^*/m_{\xi\xi_0})^{1/2}}\right] \tag{2.8}$$

Eq. (2.8) reveals that both R_s and ρ_c would decrease with electrons transferred out of p-type graphene. Placing the reported value before ($R_s \sim 1000\ \Omega/\text{sq}$ and $\rho_c = 1\ \Omega\,\text{cm}$) and after chemical doping ($R_s \sim 300\ \Omega/\text{sq}$ and $\rho_c = 0.1\ \Omega\,\text{cm}$) into the above equation, we can obtain the current diffusion length L_s after chemical doping $L_s \approx \sqrt{\rho_c/R_l} = \sqrt{0.1\ \Omega\,\text{cm}^2/300\ \Omega} = 182\ \mu m$. Even though L_s decreased after chemical doping in this case however, the contact resistance also decreased ($R = \rho_c/S = 0.1\ \Omega\,\text{cm}^2/0.01\ \text{cm}^2 = 10\ \Omega$), so the ultimately increased device V_F is comparably small ($\Delta V = RI = 3.5\ \text{V}$).

As the SLG R_s after chemical doping is still too large, multilayer graphene (MLG) is also under investigation as an alternative. Surveying the MLG TCE from a bird's-eye view, taking $R_s \sim 30\ \Omega/\text{sq}$ and $\rho_c = 0.01\ \Omega\,\text{cm}^2$, the current diffusion length L_s is determined to be 182 μm, the same order as that of chemical doped SLG. The introduced series resistance was greatly decreased ($R = \rho_c/S = 0.01\ \Omega\,\text{cm}^2/0.01\ \text{cm}^2 = 1\ \Omega$), at the cost of optical transparency (T=1-2.3% n, n being the MLG layer number). We can further understand the current flow in MLG as a resistor network (Figure S1). In-plane conductivity (σ-xy) and out-of-plane conductivity of MLG (σ-z) are assumed to be constant, and all of the current is injected into the top film. We have neglected the fact that the in-plane resistivity of the bottom layer has been reported to be larger due to the effects of the charged impurities in the substrate. L_s and L_z represent the distance the current flows in plane and out of plane, before being homogeneously distributed. Taking L_s minimum to be 150 μm, and the interlayer separation of MLG to be $a_0 = 0.34$ nm, for $L_s \gg 4.5 \times 10^5$ ($= 150\ \mu\text{m}/0.34\ \text{nm}$) L_z, MLG exhibits the same sheet conductance regardless of the number of stacked layers because of the poor interlayer conductivity (i.e., all of the current flows in the top layer, path I); for $L_s \ll 4.5 \times 10^5 L_z$, increasing the layer number adds conductive channels in parallel, therefore resulting in a decrease in R_s that is inversely proportional to the number of MLG (path II); for $L_s \sim 4.5 \times 10^5\ L_z$, R_s saturates after a certain number of layers. The L_s/L_z ratio can be estimated in terms of in-plane conductivity (σ-xy) and out-of-plane conductivity (σ-z), which is as high as $\sim 9 \times 10$ [432,33]. This indicates that stacking graphene layers essentially adds channels for charge transport and saturates after a certain number. To achieve a current diffusion length of ~150 μm, the MLG layer number can be estimated to be 5~6 ($1.50 \times 10^5\ \text{nm}/0.34\ \text{nm} \times n = 9 \times 10^4$). In a real VLEDs device (Figure 5(b)), the n-GaN layer actually serves as the additional intrinsic TCE, so the layer number of the ideal MLG TCEs n should be less than 5. Further chemical doping of MLG should further decrease R_s and ρ_c.

V-LEDs and others

We are the first to transfer graphene TCEs onto the N-polar u-GaN surface of V-LEDs [93]. All of the graphene TCEs-based V-LEDs chips show improved LOP and the average increase is about 25%. However, due to the relatively large R_c between graphene and u-GaN, V_F (4.19 V@350 mA) degrades compared with the control sample (3.96 V@350 mA). By dry etching N-polar n-GaN, combining with graphene TCEs and an HRM CBL (high reflective membrane current blocking layer) deposited on the p-GaN side, we can manipulate the current distribution and obtain the best chip results [92], which shows

60% increase in LOP and relieved EQE drop compared with the control sample. Relying on its low flexural rigidity, graphene also was used as stretchable transparent interconnections in micro-scale LEDs and V-LEDs arrays [94,95]. It can conform itself to corrugated and even bending surface, in a manner yielding intense physical contact and thus low R_c and good reliability. We have reported the in-situ fabrication of bendable micro-scale hexagonal pyramids array V-LEDs with graphene as stretchable electrical interconnects [95]. Under tensile strain while bending, the adjacent graphene sheets slide against each other; hence, the tensile strain can be easily "absorbed and canceled". Moreover, graphene can be buried during the CVD process, serving as quasi-nucleation layer [96], thermal dissipation layer [97] and transfer sacrificial layer [98].

Proposals

Although the state-of-the-art interface engineering or chemical doping has been proved to be useful when addressing the high ρ_c problem for graphene TCEs on GaN LEDs, several obvious limitations of these methods can be observed: (1) Add much more fabrication complexity, especially for the interface engineering method. (2) Generally, the above-mentioned $AuCl_3$ or HNO_3 treatment is surface doping (chemical doping includes surface transfer doping and substitutional doping), which does not modify the bulk structure and could be reversible. It also means that the doping agents can be desorbed from graphene, leading to the doping process malfunctioning. Annealing proves efficient in reducing ρ_c to some extent [63,99], yet it has its own limitations. Here we demonstrate our two proposals for graphene TCEs' utilization.

Tunnel junction (TJ) approach

The TJ approach introduces single or multiple n-doped $In_xGa_{1-x}N$ layers on the top of the p-GaN layer during local Metal organic CVD (MOCVD) growth and replaces additional deposition steps during chip processing before graphene transferring, as illustrated in Figure 4(a) and the sketched graphene-n-$In_xGa_{1-x}N$/p-GaN band diagram in Figure 4(b). The two TJ interfaces therefore include the graphene/n-$In_xGa_{1-x}N$ interface and the n-$In_xGa_{1-x}N$/p-GaN interface. An anomalous nearly ohmic (linear) current–voltage characteristic has been observed by Esaki [100] in the reverse biased TJ junction, which first revealed the quantum tunnel across the depletion region of the junction. Tunnel resistance (TR) is determined by the equivalent energy and momentum states of the electrons and holes at both the TJ sides and the tunnel distances (TD). Inferred from our calculation of graphene/GaN contacts ρ_c above [66], a lower ρ_c value could be expected between graphene and the top heavy n-doped $In_xGa_{1-x}N$ layer. This is due to the high probability of holes (electrons) tunnel from graphene ($In_xGa_{1-x}N$) to $In_xGa_{1-x}N$ (graphene), which has been described in Figure 2(d2). As to the n-$In_xGa_{1-x}N$/p-GaN

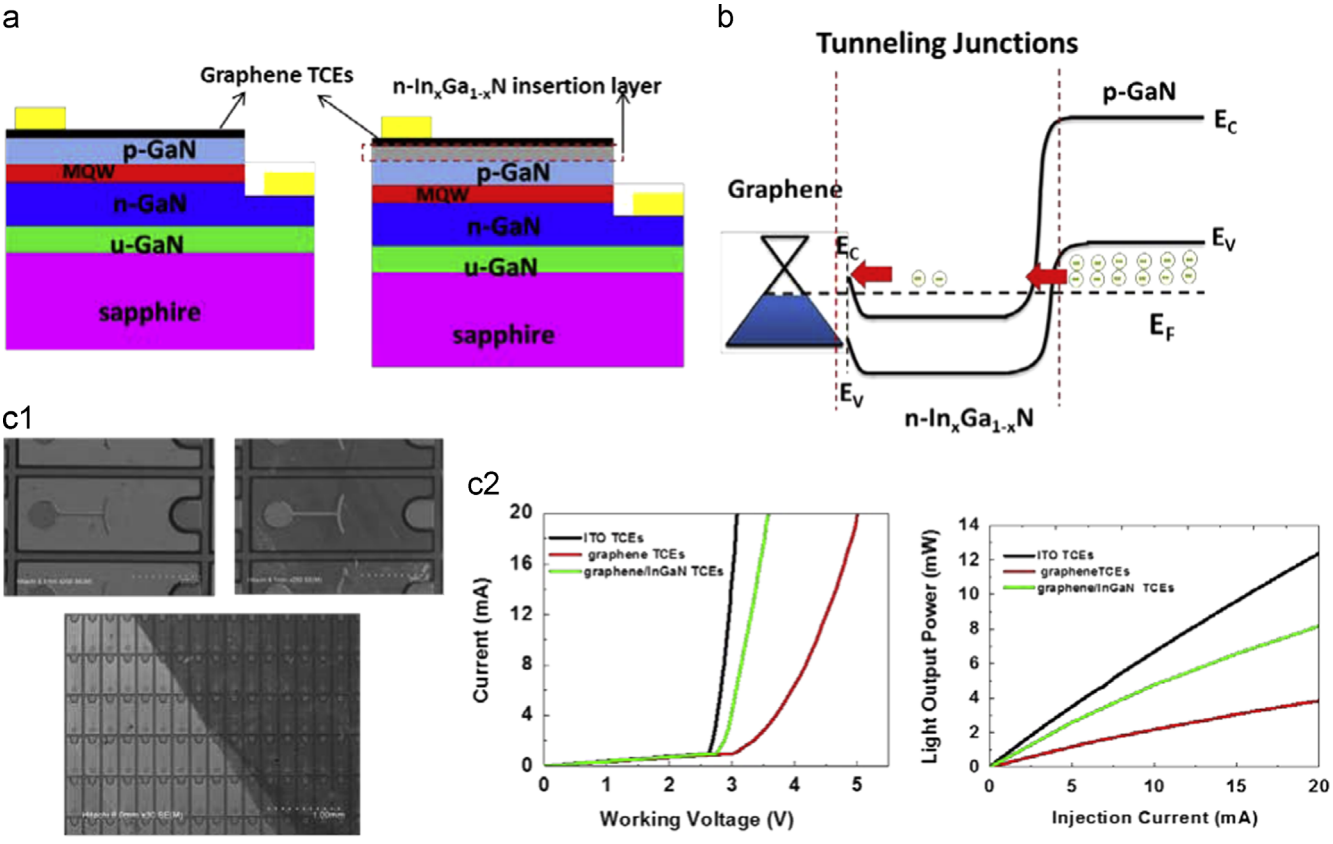

Figure 4 (a) Sketches the tunnel junction LED device design for graphene TCEs; (b) sketches n-$(In)_xGa_{1-x}N$/p-GaN band diagram; (c1) shows the top-view SEM images of LED chip after transferring graphene; and (c2) shows the *I-V* curves and I-LOP of LEDs based on conventional ITO, bare graphene and graphene–InGaN TCEs.

interface, degenerately doping will bring up E_F into the conduction band (CB). When reverse bias is applied to the n-$In_xGa_{1-x}N$/p-GaN junction (i.e. LED is forward biased), the tunnel probability for holes from valence band (VB) of p-GaN across the TJ junction will increase. Large-density intrinsic dislocations (10^8 /cm) and defects in GaN grown on sapphire also provide multiple tunnel paths for carrier transportation. In addition, as p-GaN is grown at a relatively lower temperature (960 °C) compared with n-GaN (1050 °C), a degraded material quality with higher dislocation density results, which makes it more preferable for carriers to tunnel across. As the n-$In_xGa_{1-x}N$ layer is thinner (2 nm) than the total depletion width of the two tunnel junctions, the two TJ interfaces would be connected and the n-$In_xGa_{1-x}N$ layer is totally depleted. This makes it easier for carriers to tunnel across and thus reduce the total series resistance. Although the proposed TJ design principle is simple, realizing TJ with a low TR in epitaxial growth needs effort in both growth parameter optimization and rational TJ structure. For example, because of the ionic component discrepancy in InN and GaN, a space charge will develop at the interface of GaN/InN. Behaving in the same manner as doping-induced charge, the space charge will bend the TJ bands and reduce the TD and TR. Also the narrower band gap of InN further reduces TD. Interval insertion of $In_xGa_{1-x}N$(x may be not fixed) in the TJ layer will create multiple stairs for holes trespassing [57,59,100].

Here we demonstrate proof-of-principle of our first effort for TJ-graphene TCEs for blue LEDs. A 2 nm-thick n^+-$In_xGa_{1-x}N$ layer was additionally grown on p^+-GaN, with growth temperature $T\sim744$ °C. In composition has been designed to be ~0.1 (lower than In composition in the MQWs) to prevent the re-absorption of emitted light from MQWs (with In fraction about 15%) in the top TJ layer. Figure 4(c1) shows the top-view SEM images of LED chip (a) before and (b) after transferring graphene. Figure 4(c2) shows the I-V curves and I-LOP of LEDs based on conventional ITO, bare graphene and graphene-InGaN TJ TCEs. Graphene-TJ TCEs-based LEDs exhibit lower V_F (3.58 V@20 mA) and higher LOP (8.18 mW), compared with that of bare graphene-based LEDs (5.02 V@20 mA, ~3.85 mW). Though it is still inferior to ITO-based LEDs' performance (3.08 V@20 mA, ~12.39 mW), this preliminary result shows the proposal of TJ TCEs is promising. Further optimized design of the tunnel structures and an improvement in graphene material quality can be beneficial for further enhancement of the graphene TCEs-based LED devices performance.

Graphene local growths on GaN

To date, nearly all the graphene TCEs in GaN-based LEDs mentioned above are derived through the wet-transfer CVD method, with its inherent obvious drawbacks [101]: the transfer process is very complicated and susceptible to unintentional and irreversible doping or contamination, leading to the adsorption/accumulation of residues, oxides and wrinkles at the graphene/GaN interface, and hence greatly affecting the contact properties. Also, it is quite indispensable for graphene to adhere strongly to the target substrate. Koenig [102] found an adhesion energy of 0.45 ± 0.02 J m^{-2} for monolayer graphene and 0.31 ± 0.02 J m^{-2} for two-to-five layered sheets. Yoon [103] et al. found the adhesion energy of monolayer graphene as grown on copper to be 0.72 ± 0.07 J m^{-2}. Both results suggest ultrastrong adhesion of graphene membranes due to intrinsic graphene mechanical properties and graphene/substrate interface electron redistribution. Indeed, strong adhesion is very important for chip fabrication, performance and reliability. Ideally, for SLG, according to theoretical prediction and experimental results [102,103], it shows a strong adhesion with the underlying substrate. However, for bilayer graphene and MLG, carbon atoms between the layers are held together by relatively weak van der Waals forces, thus making them prone to cleavage, and peeling off together with the top metal contact, even though the bottom layer in bilayer graphene and MLG can adhere strongly to the substrate [102]. However, we found that in our chip fabrication process, graphene is very fragile and extremely prone to be exfoliated or broken, especially in metal lift-off and cleaning processes (Figure 5(a), exfoliated graphene with PMMA), contrasting with the result found by Steven P. Koenig and Taeshik Yoon. We assume the poor adhesion arises from wet-transfer process. For wet-transferred SLG or MLG, if there are some residues at the bottom, the risk for peeling off of graphene TCEs together with the residue will increase. Further, bearing an unaffordable high consumption of energy and time, the cost of graphene CVD and transfer process is yet to be reduced to be competitive in widespread applications. It is of great significance to develop a reproductive, reliable and feasible technique to grow graphene directly on the target substrate (such as Si, GaN, GaAs, etc.). We think this is the ultimate solution for graphene TCEs and widespread applications.

The mechanisms for CVD graphene precipitation have been well understood and verified in many transition metals [20,104-108] (belonging to the group VIII metals) and catalytic carbides of transition metals [109] (such as TaC, WC, TiC, HfC and LaB_3), with Ni and Cu as two typical representatives. For Ni, Ni_3C solid solution is formed at elevated temperature and the solubility decreases while temperature decreases, resulting in the precipitation of carbon into graphene. For Cu, it has very low carbon solubility and just acts as a catalyst. This is attributed to the metal d-orbitals differentiation, surprisingly coinciding with metal/graphene contacts introduced above: partially d-orbitals filled metals (such as Ni$3d^84s^2$, Co$3d^74s^2$, Fe$3d^64s^2$) are capable of providing low-energy pathways for chemical interaction or appropriate intermediates formation with carbon, in both CVD growth and contact conditions; conversely, metal with full or half-filled d-orbitals (as Cu $3d^{10}4s^1$) can only form soft bonds with carbon via charge transfer from d-orbitals to the empty s states, acting as a true catalyst for graphene formation. By placing solid carbon source (PMMA) onto or in between Ni/ insulating substrates, Tour's group [110,111] has successfully demonstrated bilayer graphene CVD growth through carbon diffusion out of Ni.

Taking these experiences for CVD graphene on GaN, some critical issues should be addressed. Different from inert insulating substrate, e.g., SiO_2 and Si_3N_4, GaN is more likely to decompose at elevated temperature, especially for GaN-based LEDs with InGaN/GaN MQWs; high temperature will lead to In segregation and hence influence the emission properties. C_2H_2, which has a lower decomposition temperature, is recommended as the carbon precursor, instead of conventional CH_4. Additionally, the mechanism for CVD graphene growth on non-

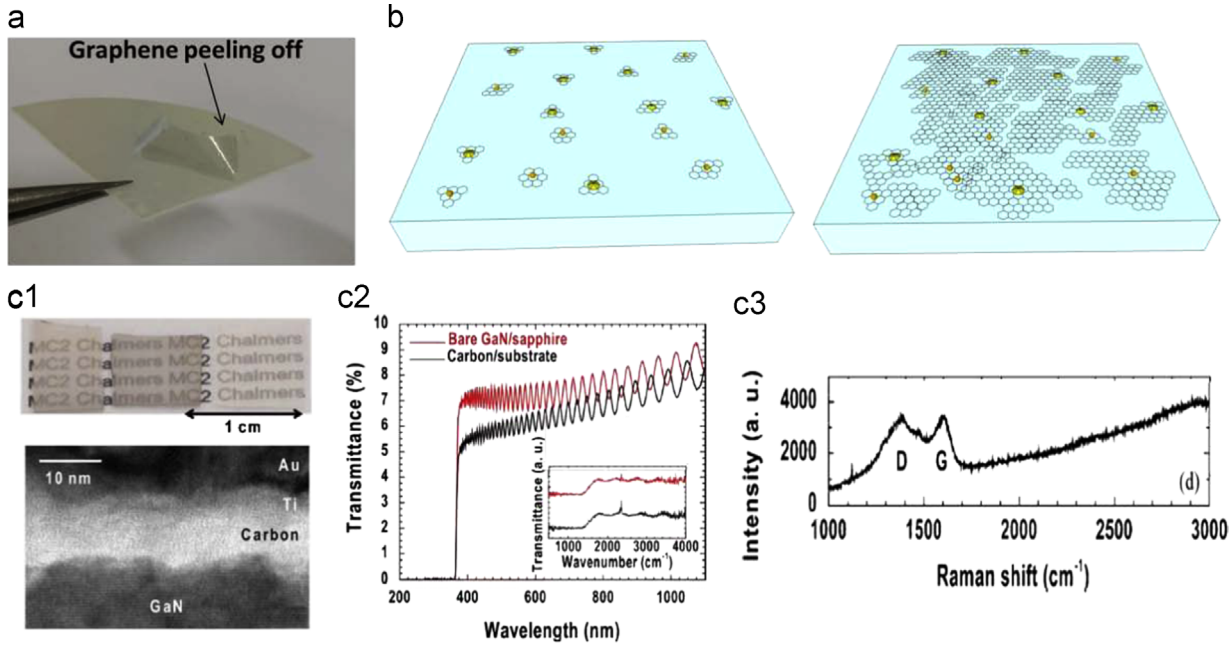

Figure 5 (a) Micrograph of exfoliated wet-transferred graphene (with PMMA) on GaN substrate; (b) sketches the growth mechanism of graphene on GaN; (c1 up) [121] carbon thin films on GaN/sapphire (left two) and the bare substrate (right), (c1 lower) high-resolution cross-section TEM micrograph of a carbon/GaN sample, where the carbon thin film is intentionally grown thicker for easy detection of the graphitic layers; (c2) UV–vis–NIR transmittance of the carbon thin film and the bare GaN/sapphire. The carbon thin film absorbs ~2% of the incident light. Inset: FTIR spectra of the same samples, which have been shifted along the ordinate for clarity; and (c3) Raman spectra (514 nm, 0.5 mW) of the as-grown carbon thin film on GaN. Copyright from IEEE.

metallic substrates is still obscure, whether it is catalytic or not. Recent advances in graphene grown on non-metallic substrates include CVD on hafnium dioxide [112,113] (HfO_2), sapphire [114], SiO_2[115], Si_3N_4 [116], BN, MgO [117], ZnS, etc. Sun [114] suggests a non-catalytic self-assembly process of carbon cluster. Scott [118] emphasizes the importance of step sites of the non-metallic substrates, which anchor the carbon nano-flakes and serve as nucleation sites, resembling the conventional step-flow CVD process.

Based on the experiences both from others and from our group, we think graphene CVD on GaN is a combination of catalytic and non-catalytic processes. Figure 5(b) sketches the growth mechanism of graphene on GaN. MOCVD-grown GaN surface often displays a lack of N atoms and excessive of Ga atoms. The elevated temperature will make the Ga atom more dominant due to GaN decomposition [119]. Inferred from the mechanism of CVD graphene growth on Cu, a metal Ga with full occupied d-orbital ($3d^{10}4S^24P^1$) catalytic process is possible. Actually, Ga and carbon are known to be an insoluble system, similar to Cu (with quite low affinity with carbon), further supporting the above analysis [120,121]. Although the GaN-graphene bonding type is basically van der Waals adhesion, we believe the interatomic force between GaN and locally grown graphene is stronger than that via wet transfer methods due to a stronger bonding between metal Ga and carbon atoms [103]. Moreover, due to the state-of-the-art MOCVD GaN growth (on sapphire substrate) technology and especially the lowered growth temperature of the top p-GaN, the p-GaN surface typically exhibits random distributed hexagonal pits, which serve as the favorable sites for carbon source dissociation and carbon nucleation. However, this also makes the deposited carbon layer non-uniform, in contrast with those on inert substrates such as Si_3N_4 and SiO_2.

Sun [122] has demonstrated the first result of CVD-grown large-area carbon thin film on GaN at 950 °C and 750mbar for 5 min in a flow of 160 sccm C_2H_2 and 1000sccm NH_3. Low-decomposition-temperature C_2H_2 as the precursor and an overpressure of NH_3 were chosen in order to protect the GaN surface from dissociating. The as-grown film shows ~6.7 nm thickness (Figure 5(c1)) and abnormal ~2% transmittance (Figure 5(c2)), and is more resistive than expected. Yet the absence of 2d peak in the Raman spectrum (Figure 5(c3)) and the detailed refraction TEM results (Figure 5(b1)) indicate the as-grown film may be a combination of graphene sheets and some other carbon film allotropes. Specifically, for graphene TCEs' application on lateral LEDs, we propose a combination with the TJ scheme: local growth of graphene on the n-In_xGaN_{1-x}/p-GaN-MQW-n-GaN layer. This should result in a relatively lower contact resistance and strong adhesion simultaneously. Much effort still needs to be devoted for scalable, continuous, uniform and thickness and some other properties (e.g. doping) controllable graphene TCEs deposition directly on GaN-based LEDs. The inner mechanism deserves more deep investigations.

Reliability of graphene TCEs for GaN-based LEDs

The reliability of graphene TCEs for GaN-based LEDs undoubtedly needs equal attention, yet there are few reports on it to

date. Kim [123] reported the severe degradation of graphene TCEs when the UV LEDs were continuously biased for 30 s at a bias of 10 V. There was less degradation when the UV-LED was operated at a pulsed bias condition with 5% duty cycle for totally 30 s. It indicates that the high junction temperature and joule heating caused oxidation of the graphene TCEs, which are accountable for its degradation. Liu [124] found that the O_2 etching kinetics varies strongly with the number of graphene layers. Oxidation of triple layers is similar to the natural graphite and HOPG, featured with uniformly sized one-layer-deep etch pits, which is initiated at preexisting point defects, followed by constant radial growth. In contrast to the triple layers, SLG and bilayer graphene are more reactive to O_2: featured with one-layer-deep or two-layer-deep etch pits, oxygen-atom attack can nucleate and grow etch pits on even a defect-free basal plane, as well as at preexisting defects. Further refer to the reports of graphene reliability in other devices, such as Field-Effect Transistors (FET) [125–127] and supercapacitors [128,129]; the possible degradation mechanism for graphene TCEs in GaN-based LEDs can be: degradation from the graphene itself, the graphene/GaN contacts and GaN/metal contact. The heating and cooling cycles can make graphene TCEs structurally deformed, showing regions of curvature and domains of lower than hexagonal symmetry, resulting in some sp^3 C orbital character and π-orbital misalignment. This is expected to lead to degradation in graphene mobility and significantly increased reactivity with O_2. The generated heat also accelerates the graphene TCEs' oxidation process, which can severely degrade the graphene and thus LEDs' optical and electrical characteristics [122]. Aging under environmental exposure, intrinsic graphene acoustic phonon scattering, Coulomb impurities, surface roughness and surface polar phonon scattering could lead to mobility degradation of graphene [126]. The interfacial impurity scattering (e.g. Mg^{2+} in p-GaN) could degrade the mobility of graphene and graphene/GaN contact resistance [125]. Electromigration (EM) is another issue to be considered. The current-induced thermal annealing makes the electrons gain certain energy, atoms become separated from the interface and are transported in the direction of the current. This will increase the metal/GaN contact resistance and even make the graphene TCEs electrical interconnect fail [128].

Conclusions

We have presented a review of the state-of-art graphene TCEs used in GaN-based LEDs. The electronic and optical properties of graphene have been reviewed. Graphene/GaN contacts then were analyzed and discussed in detail. Self-adaptive and reverse bias doping of graphene E_F, as well as carriers' tunnel are considered to be responsible for the relatively lower barrier heights of the graphene/GaN interface. Current approaches, including interface engineering, chemical doping and tunnel junction design for graphene TCEs utilization in LEDs and the corresponding chip results have been summarized. For overcoming the obvious complexity and fragile drawbacks of the wet-etching transfer method, graphene directly grown on GaN by the CVD method was strongly recommended and introduced in detail. Finally, we provide a short analysis on the reliability of graphene TCEs for GaN-based LEDs. We think that graphene directly grown on GaN by CVD combined with tunnel junction design could be the ultimate countermeasure to obtain low series resistance (contact resistance included), fabrication compatibility and reliable adhesion, paving the way for the ultimate application of graphene TCEs in GaN-based LEDs and in general of other opto- and electrical devices.

Acknowledgment

This work was supported by the National Research Foundation of Singapore under Grant no. NRF-CRP-6-2010-2, NRF-RF-2009-09, the Singapore Agency for Science, Technology and Research (A*STAR) SERC under Grant no. 112 120 2009 and the National High Technology Program of China (Grant no. 2013AA03A101), the National Natural Science Foundation of China (Grant nos. 51372133, 61306050 and 61306051).

Appendix A. Supporting information

Supplementary data associated with this article can be found in the online version at http://dx.doi.org/10.1016/j.nanoen.2014.12.035.

References

[1] S. Nakamura, Science 281 (5379) (1998) 956–961.
[2] P. Waltereit, O. Brandt, A. Trampert, H.T. Grahn, J. Menniger, M. Ramsteiner, M. Reiche, K.H. Ploog, Nature 406 (6798) (2000) 865–868.
[3] Z. Liu, T. Wei, E. Guo, X. Yi, L. Wang, J. Wang, G. Wang, Y. Shi, I. Ferguson, J. Li, Appl. Phys. Lett. 99 (9) (2011) 091104.
[4] J.K. Kim, S. Chhajed, M.F. Schubert, E.F. Schubert, A.J. Fischer, M.H. Crawford, J. Cho, H. Kim, C. Sone, Adv. Mater. 20 (4) (2008) 801–804.
[5] S.-J. Wang, K.-M. Uang, S.-L. Chen, Y.-C. Yang, S.-C. Chang, T.-M. Chen, C.-H. Chen, B.-W. Liou, Appl. Phys. Lett. 87 (1) (2005) 011111.
[6] Y. Zhang, H. Zheng, E. Guo, Y. Cheng, J. Ma, L. Wang, Z. Liu, X. Yi, G. Wang, J. Li, J. Appl. Phys. 113 (1) (2013) 014502.
[7] D.W. Kim, H.Y. Lee, M.C. Yoo, G.Y. Yeom, Appl. Phys. Lett. 86 (5) (2005) 052108.
[8] A.K. Geim, K.S. Novoselov, Nat. Mater. 6 (3) (2007) 183–191.
[9] F. Bonaccorso, Z. Sun, T. Hasan, A.C. Ferrari, Nat. Photonics 4 (9) (2010) 611–622.
[10] P. Matyba, H. Yamaguchi, M. Chhowalla, N.D. Robinson, L. Edman, ACS Nano 5 (1) (2010) 574–580.
[11] Y.-M. Lin, C. Dimitrakopoulos, K.A. Jenkins, D.B. Farmer, H.-Y. Chiu, A. Grill, P. Avouris, Science 327 (5966) (2010) 662.
[12] X. Li, H. Zhu, K. Wang, A. Cao, J. Wei, C. Li, Y. Jia, Z. Li, X. Li, D. Wu, Adv. Mater. 22 (25) (2010) 2743–2748;
B. Xia, Y. Yan, X. Wang, X.W. Lou, Mater. Horiz. 1 (4) (2014) 379–399.
[13] P.R. Wallace, Phys. Rev. 71 (9) (1947) 622–634.
[14] A.H. Castro Neto, F. Guinea, N.M.R. Peres, K.S. Novoselov, A.K. Geim, Rev. Mod. Phys. 81 (1) (2009) 109–162.
[15] G.W. Semenoff, Phys. Rev. Lett. 53 (26) (1984) 2449–2452.
[16] R.R. Nair, P. Blake, A.N. Grigorenko, K.S. Novoselov, T.J. Booth, T. Stauber, N.M.R. Peres, A.K. Geim, Science 320 (5881) (2008) 1308.
[17] P. Blake, P.D. Brimicombe, R.R. Nair, T.J. Booth, D. Jiang, F. Schedin, L.A. Ponomarenko, S.V. Morozov, H.F. Gleeson,

E.W. Hill, A.K. Geim, K.S. Novoselov, Nano Lett. 8 (6) (2008) 1704–1708.
[18] A. Reina, X. Jia, J. Ho, D. Nezich, H. Son, V. Bulovic, M.S. Dresselhaus, J. Kong, Nano Lett. 9 (1) (2008) 30–35.
[19] X. Li, Y. Zhu, W. Cai, M. Borysiak, B. Han, D. Chen, R.D. Piner, L. Colombo, R.S. Ruoff, Nano Lett. 9 (12) (2009) 4359–4363.
[20] X. Li, W. Cai, J. An, S. Kim, J. Nah, D. Yang, R. Piner, A. Velamakanni, I. Jung, E. Tutuc, S.K. Banerjee, L. Colombo, R.S. Ruoff, Science 324 (5932) (2009) 1312–1314.
[21] H. Bi, F. Huang, J. Liang, X. Xie, M. Jiang, Adv. Mater. 23 (28) (2011) 3202–3206.
[22] Q. Yu, L.A. Jauregui, W. Wu, R. Colby, J. Tian, Z. Su, H. Cao, Z. Liu, D. Pandey, D. Wei, T.F. Chung, P. Peng, N.P. Guisinger, E.A. Stach, J. Bao, S.-S. Pei, Y.P. Chen, Nat. Mater. 10 (6) (2011) 443–449.
[23] S.Y. Jeong, S.H. Kim, J.T. Han, H.J. Jeong, S. Yang, G.-W. Lee, ACS Nano 5 (2) (2011) 870–878.
[24] H.A. Becerril, J. Mao, Z. Liu, R.M. Stoltenberg, Z. Bao, Y. Chen, ACS Nano 2 (3) (2008) 463–470.
[25] S. Gilje, S. Han, M. Wang, K.L. Wang, R.B. Kaner, Nano Lett. 7 (11) (2007) 3394–3398.
[26] X. Wang, L. Zhi, K. Mullen, Nano Lett. 8 (1) (2007) 323–327.
[27] V.C. Tung, M.J. Allen, Y. Yang, R.B. Kaner, Nat. Nano 4 (1) (2009) 25–29.
[28] G. Eda, G. Fanchini, M. Chhowalla, Nat. Nano 3 (5) (2008) 270–274.
[29] S. Bae, H. Kim, Y. Lee, X. Xu, J.-S. Park, Y. Zheng, J. Balakrishnan, T. Lei, H. Ri Kim, Y.I. Song, Y.-J. Kim, K.S. Kim, B. Ozyilmaz, J.-H. Ahn, B.H. Hong, S. Iijima, Nat. Nano 5 (8) (2010) 574–578.
[30] Q. Zheng, W.H. Ip, X. Lin, N. Yousefi, K.K. Yeung, Z. Li, J.-K. Kim, ACS Nano 5 (7) (2011) 6039–6051.
[31] I. Khrapach, F. Withers, T.H. Bointon, D.K. Polyushkin, W.L. Barnes, S. Russo, M.F. Craciun, Adv. Mater. 24 (21) (2012) 2844–2849.
[32] K. Kim, H.J. Park, B.-C. Woo, K.J. Kim, G.T. Kim, W.S. Yun, Nano Lett. 8 (10) (2008) 3092–3096.
[33] I.N. Kholmanov, C.W. Magnuson, A.E. Aliev, H. Li, B. Zhang, J.W. Suk, L.L. Zhang, E. Peng, S.H. Mousavi, A.B. Khanikaev, R. Piner, G. Shvets, R.S. Ruoff, Nano Lett. 12 (11) (2012) 5679–5683.
[34] G. Giovannetti, P. Khomyakov, G. Brocks, V. Karpan, J. van den Brink, P. Kelly, Phys. Rev. Lett. 101 (2) (2008).
[35] Q. Ran, M. Gao, X. Guan, Y. Wang, Z. Yu, Appl. Phys. Lett. 94 (10) (2009) 103511.
[36] K.T. Chan, J.B. Neaton, M.L. Cohen, Phys. Rev. B 77 (23) (2008) 235430.
[37] E. Watanabe, A. Conwill, D. Tsuya, Y. Koide, Diam. Relat. Mater. 24 (0) (2012) 171–174.
[38] E.J. Lee, K. Balasubramanian, R.T. Weitz, M. Burghard, K. Kern, Nat. Nanotechnol. 3 (8) (2008) 486–490.
[39] A. Venugopal, L. Colombo, E.M. Vogel, Appl. Phys. Lett. 96 (1) (2010) 013512.
[40] F. Xia, V. Perebeinos, Y.-m. Lin, Y. Wu, P. Avouris, Nat. Nano 6 (3) (2011) 179–184.
[41] P.A. Khomyakov, G. Giovannetti, P.C. Rusu, G. Brocks, J. van den Brink, P.J. Kelly, Phys. Rev. B 79 (19) (2009).
[42] B. Huard, N. Stander, J. Sulpizio, D. Goldhaber-Gordon, Phys. Rev. B 78 (12) (2008).
[43] X. Ji, J. Zhang, Y. Wang, H. Qian, Z. Yu, Phys. Chem. Chem. Phys. 15 (41) (2013) 17883–17886.
[44] S. Tongay, M. Lemaitre, X. Miao, B. Gila, B.R. Appleton, A.F. Hebard, Phys. Rev. X 2 (1) (2012) 011002.
[45] S. Tongay, M. Lemaitre, T. Schumann, K. Berke, B.R. Appleton, B. Gila, A.F. Hebard, Appl. Phys. Lett. 99 (10) (2011) 102102.
[46] H. Zhong, Z. Liu, G. Xu, Y. Fan, J. Wang, X. Zhang, L. Liu, K. Xu, H. Yang, Appl. Phys. Lett. 100 (12) (2012) 122108.
[47] L. Wang, Y. Zhang, X. Li, E. Guo, Z. Liu, X. Yi, H. Zhu, G. Wang, RSC Adv. 3 (10) (2013) 3359.
[48] S. Kurtin, T.C. McGill, C.A. Mead, Phys. Rev. Lett. 22 (26) (1969) 1433–1436.
[49] L.F. Lester, J.M. Brown, J.C. Ramer, L. Zhang, S.D. Hersee, J.C. Zolper, Appl. Phys. Lett. 69 (18) (1996) 2737.
[50] S.M. Sze, K.K. Ng, Physics of Semiconductor Devices, 3rd ed., Wiley, Hoboken, 2007.
[51] Y.-J. Yu, Y. Zhao, S. Ryu, L.E. Brus, K.S. Kim, P. Kim, Nano Lett. 9 (10) (2009) 3430–3434.
[52] C.Y. Su, D. Fu, A.Y. Lu, K.K. Liu, Y. Xu, Z.Y. Juang, L.J. Li, Nanotechnology 22 (18) (2011) 185309.
[53] R.T. Tung, Phys. Rev. B 64 (20) (2001) 205310.
[54] R.T. Tung, Mater. Sci. Eng.: R: Rep. 35 (1–3) (2001) 1–138.
[55] R. Tung, Phys. Rev. B 64 (20) (2001).
[56] C. Gong, D. Hinojos, W. Wang, N. Nijem, B. Shan, R.M. Wallace, K. Cho, Y.J. Chabal, ACS Nano 6 (6) (2012) 5381–5387.
[57] L.S. Yu, Q.Z. Liu, Q.J. Xing, D.J. Qiao, S.S. Lau, J. Redwing, J. Appl. Phys. 84 (4) (1998) 2099.
[58] G. Gomila, O.M. Bulashenko, J.M. Rubí, J. Appl. Phys. 83 (5) (1998) 2619.
[59] X.A. Cao, E.B. Stokes, P.M. Sandvik, S.F. LeBoeuf, J. Kretchmer, D. Walker, Electron Device Lett. IEEE 23 (9) (2002) 535–537.
[60] T. Metzger, R. Höpler, E. Born, O. Ambacher, M. Stutzmann, R. Stömmer, M. Schuster, H. Göbel, S. Christiansen, M. Albrecht, H.P. Strunk, Philos. Mag. A 77 (4) (1998) 1013–1025.
[61] X. Li, L. Fan, Z. Li, K. Wang, M. Zhong, J. Wei, D. Wu, H. Zhu, Adv. Energy Mater. 2 (4) (2012) 425–429.
[62] E. Shi, H. Li, L. Yang, L. Zhang, Z. Li, P. Li, Y. Shang, S. Wu, X. Li, J. Wei, K. Wang, H. Zhu, D. Wu, Y. Fang, A. Cao, Nano Lett. 13 (4) (2013) 1776–1781.
[63] S. Chandramohan, J.H. Kang, B.D. Ryu, J.H. Yang, S. Kim, H. Kim, J.B. Park, T.Y. Kim, B.J. Cho, E.K. Suh, C.H. Hong, ACS Appl. Mater. Interfaces 5 (3) (2013) 958–964.
[64] A. Das, S. Pisana, B. Chakraborty, S. Piscanec, S.K. Saha, U.V. Waghmare, K.S. Novoselov, H.R. Krishnamurthy, A.K. Geim, A.C. Ferrari, A.K. Sood, Nat. Nano 3 (4) (2008) 210–215.
[65] W.J.R. Hoefer, Microwave theory and techniques, IEEE Trans. 33 (10) (1985) 882–893.
[66] L. Wang, Y. Zhang, X. Li, Z. Liu, E. Guo, X. Yi, J. Wang, H. Zhu, G. Wang, J.Phys. D Appl. Phys. 45 (50) (2012) 505102.
[67] L. Wang, Z. Liu, E. Guo, H. Yang, X. Yi, G. Wang, ACS Appl. Mater. Interfaces 5 (12) (2013) 5797–5803.
[68] H.-M. Huang, C.-Y. Chang, Y.-S. Hsu, T.-C. Lu, Y.-P. Lan, W.-C. Lai, Appl. Phys. Lett. 101 (6) (2012) 061905.
[69] G. Jo, M. Choe, C.Y. Cho, J.H. Kim, W. Park, S. Lee, W.K. Hong, T.W. Kim, S.J. Park, B.H. Hong, Y.H. Kahng, T. Lee, Nanotechnology 21 (17) (2010) 175201.
[70] T.H. Seo, T.S. Oh, S.J. Chae, A.H. Park, K.J. Lee, Y.H. Lee, E.-K. Suh, Jpn. J. Appl. Phys. 50 (2011) 125103.
[71] B.-J. Kim, C. Lee, Y. Jung, K. Hyeon Baik, M.A. Mastro, J.K. Hite, C.R. Eddy, J. Kim, Appl. Phys. Lett. 99 (14) (2011) 143101.
[72] B.-J. Kim, M.A. Mastro, J. Hite, C.R. Eddy, J. Kim, Opt. Express 18 (22) (2010) 23030–23034.
[73] B.-J. Kim, G. Yang, M. Joo Park, J. Seop Kwak, K. Hyeon Baik, D. Kim, J. Kim, Appl. Phys. Lett. 102 (16) (2013) 161902.

[74] J.-P. Shim, T. Hoon Seo, J.-H. Min, C. Mo Kang, E.-K. Suh, D.-S. Lee, Appl. Phys. Lett. 102 (15) (2013) 151115.
[75] Y. Zhang, X. Li, L. Wang, X. Yi, D. Wu, H. Zhu, G. Wang, Nanoscale 4 (19) (2012) 5852–5855.
[76] T.H. Seo, K.J. Lee, T.S. Oh, Y.S. Lee, H. Jeong, A.H. Park, H. Kim, Y.R. Choi, E.-K. Suh, T.V. Cuong, V.H. Pham, J.S. Chung, E.J. Kim, Appl. Phys. Lett. 98 (25) (2011) 251114.
[77] X. Kun, X. Chen, D. Jun, Z. Yanxu, G. Weiling, M. Mingming, Z. Lei, S. Jie, Appl. Phys. Lett. 102 (16) (2013) 162102.
[78] P. Kumar, L.S. Panchakarla, S.V. Bhat, U. Maitra, K.S. Subrahmanyam, C.N. Rao, Nanotechnology 21 (38) (2010) 385701.
[79] J. Min Lee, J. Yi, W. Woo Lee, H. Yong Jeong, T. Jung, Y. Kim, W. Il Park, Appl. Phys. Lett. 100 (6) (2012) 061107.
[80] T.H. Seo, A.H. Park, G.H. Lee, M.J. Kim, E.-K. Suh, J. Phys. D: Appl. Phys. 47 (31) (2014) 315102.
[81] J.P. Shim, D. Kim, M. Choe, T. Lee, S.J. Park, D.S. Lee, Nanotechnology 23 (25) (2012) 255201.
[82] T. Hoon Seo, B. Kyoung Kim, G. Shin, C. Lee, M. Jong Kim, H. Kim, E.-K. Suh, Appl. Phys. Lett. 103 (5) (2013) 051105.
[83] Z. Li, J. Kang, Z. Liu, C. Du, X. Lee, X. Li, L. Wang, X. Yi, H. Zhu, G. Wang, AIP Adv. 3 (4) (2013) 042134.
[84] M. Choe, C.-Y. Cho, J.-P. Shim, W. Park, S.K. Lim, W.-K. Hong, B. Hun Lee, D.-S. Lee, S.-J. Park, T. Lee, Appl. Phys. Lett. 101 (3) (2012) 031115.
[85] T.H. Seo, S.J. Chae, B.K. Kim, G. Shin, Y.H. Lee, E.-K. Suh, Appl. Phys. Express 5 (11) (2012) 115101.
[86] C.-Y. Cho, M. Choe, S.-J. Lee, S.-H. Hong, T. Lee, W. Lim, S.-T. Kim, S.-J. Park, J. Appl. Phys. 113 (11) (2013) 113102.
[87] H. Liu, Y. Liu, D. Zhu, J. Mater. Chem. 21 (10) (2011) 3335.
[88] Y. Shi, K.K. Kim, A. Reina, M. Hofmann, L.-J. Li, J. Kong, ACS Nano 4 (5) (2010) 2689–2694.
[89] A. Kasry, M.A. Kuroda, G.J. Martyna, G.S. Tulevski, A.A. Bol, ACS Nano 4 (7) (2010) 3839–3844.
[90] S. Chandramohan, J. Hye Kang, Y.S. Katharria, N. Han, Y. Seon Beak, K. Bok, Ko, J. Bae Park, H. Kyu Kim, E.-K. Suh, C.-H. Hong, Appl. Phys. Lett. 100 (2) (2012) 023502.
[91] S. Chandramohan, J.H. Kang, Y.S. Katharria, N. Han, Y.S. Beak, K.B. Ko, J.B. Park, B.D. Ryu, H.K. Kim, E.-K. Suh, C.-H. Hong, J. Phys. D: Appl. Phys. 45 (14) (2012) 145101.
[92] L. Wang, Y. Zhang, X. Li, Z. Liu, L. Zhang, E. Guo, X. Yi, H. Zhu, G. Wang, Proc. R. Soc. A: Math. Phys. Eng. Sci. 469 (2151) (2013) 20120652.
[93] L. Wang, Y. Zhang, X. Li, Z. Liu, E. Guo, X. Yi, J. Wang, H. Zhu, G. Wang, Appl. Phys. Lett. 101 (6) (2012) 061102.
[94] R.H. Kim, M.H. Bae, D.G. Kim, H. Cheng, B.H. Kim, D.H. Kim, M. Li, J. Wu, F. Du, H.S. Kim, S. Kim, D. Estrada, S.W. Hong, Y. Huang, E. Pop, J.A. Rogers, Nano Lett. 11 (9) (2011) 3881–3886.
[95] J. Kang, Z. Li, H. Li, Z. Liu, X. Li, X. Yi, P. Ma, H. Zhu, G. Wang, Appl. Phys. Express 6 (7) (2013) 072102;
L. Wang, J. Ma, Z. Liu, X. Yi, H. Zhu and G. Wang, ACS Photonics 1 (2014) 421-429, http://dx.doi.org/10.1021/ph500133w.
[96] C.H. Lee, Y.J. Kim, Y.J. Hong, S.R. Jeon, S. Bae, B.H. Hong, G.C. Yi, Adv. Mater. 23 (40) (2011) 4614–4619.
[97] N. Han, T.V. Cuong, M. Han, B.D. Ryu, S. Chandramohan, J.B. Park, J.H. Kang, Y.J. Park, K.B. Ko, H.Y. Kim, H.K. Kim, J.H. Ryu, Y.S. Katharria, C.J. Choi, C.H. Hong, Nat. Commun. 4 (2013) 1452.
[98] K. Chung, C.H. Lee, G.C. Yi, Science 330 (6004) (2010) 655–657.
[99] Y. Zhang, L. Wang, X. Li, X. Yi, N. Zhang, J. Li, H. Zhu, G. Wang, J. Appl. Phys. 111 (11) (2012) 114501.
[100] L.L. Chang, Appl. Phys. Lett. 24 (12) (1974) 593.
[101] K. Joo, S.K. Jerng, Y.S. Kim, B. Kim, S. Moon, D. Moon, G.D. Lee, Y.K. Song, S.H. Chun, E. Yoon, Nanotechnology 23 (42) (2012) 425302.
[102] S.P. Koenig, N.G. Boddeti, M.L. Dunn, J.S. Bunch, Nat. Nano 6 (9) (2011) 543–546.
[103] T. Yoon, W.C. Shin, T.Y. Kim, J.H. Mun, T.S. Kim, B.J. Cho, Nano Lett. 12 (3) (2012) 1448–1452.
[104] C. Mattevi, H. Kim, M. Chhowalla, J. Mater. Chem. 21 (10) (2011) 3324–3334.
[105] K.S. Kim, Y. Zhao, H. Jang, S.Y. Lee, J.M. Kim, K.S. Kim, J.H. Ahn, P. Kim, J.Y. Choi, B.H. Hong, Nature 457 (7230) (2009) 706–710.
[106] A. Grüneis, K. Kummer, D.V. Vyalikh, New J. Phys. 11 (7) (2009) 073050.
[107] M. Zheng, K. Takei, B. Hsia, H. Fang, X. Zhang, N. Ferralis, H. Ko, Y.-L. Chueh, Y. Zhang, R. Maboudian, A. Javey, Appl. Phys. Lett. 96 (6) (2010) 063110.
[108] A.T. N'Diaye, M. Engler, C. Busse, D. Wall, N. Buckanie, F.-J. Meyer, Z.U. Heringdorf, R. van Gastel, B. Poelsema, T. Michely, New J. Phys. 11 (2) (2009) 023006.
[109] T. Aizawa, R. Souda, S. Otani, Y. Ishizawa, C. Oshima, Phys. Rev. Lett. 64 (7) (1990) 768–771.
[110] Z. Peng, Z. Yan, Z. Sun, J.M. Tour, ACS Nano 5 (10) (2011) 8241–8247.
[111] Z. Yan, Z. Peng, Z. Sun, J. Yao, Y. Zhu, Z. Liu, P.M. Ajayan, J.M. Tour, ACS Nano 5 (10) (2011) 8187–8192.
[112] S. Jie, E. Lind, I. Maximov, H.Q. Xu, Electron Device Lett. IEEE 32 (2) (2011) 131–133.
[113] J. Sun, M. Larsson, I. Maximov, H.Q. Xu, Appl. Phys. Lett. 96 (16) (2010) 162107.
[114] J. Sun, M.T. Cole, N. Lindvall, K.B.K. Teo, A. Yurgens, Appl. Phys. Lett. 100 (2) (2012) 022102.
[115] J. Sun, N. Lindvall, M.T. Cole, T. Wang, T.J. Booth, P. Bøggild, K.B.K. Teo, J. Liu, A. Yurgens, J. Appl. Phys. 111 (4) (2012) 044103.
[116] J. Sun, N. Lindvall, M.T. Cole, K.B.K. Teo, A. Yurgens, Appl. Phys. Lett. 98 (25) (2011) 252107.
[117] M.H. Rümmeli, A. Bachmatiuk, A. Scott, F. Börrnert, J.H. Warner, V. Hoffman, J.-H. Lin, G. Cuniberti, B. Büchner, ACS Nano 4 (7) (2010) 4206–4210.
[118] A. Scott, A. Dianat, F. Börrnert, A. Bachmatiuk, S. Zhang, J.H. Warner, E. Borowiak-Paleń, M. Knupfer, B. Büchner, G. Cuniberti, M.H. Rümmeli, Appl. Phys. Lett. 98 (7) (2011) 073110.
[119] D. Ehrentraut, E. Meissner, M. Bockowski, Technology of Gallium Nitride Crystal Growth, Springer.
[120] J.-i. Fujita, R. Ueki, Y. Miyazawa, T. Ichihashi, J. Vac. Sci. Technol. B: Microelectron. Nanometer Struct. 27 (6) (2009) 3063.
[121] H. Hiura, M.V. Lee, A.V. Tyurnina, K. Tsukagoshi, Carbon 50 (14) (2012) 5076–5084.
[122] J. Sun, M.T. Cole, S.A. Ahmad, O. Backe, T. Ive, M. Loffler, N. Lindvall, E. Olsson, K.B.K. Teo, L. Johan, A. Larsson, A. Yurgens, A. Haglund, Semicond. Manuf. IEEE Trans. 25 (3) (2012) 494–501.
[123] B.-J. Kim, C. Lee, M.A. Mastro, J.K. Hite, C.R. Eddy, F. Ren, S.J. Pearton, J. Kim, Appl. Phys. Lett. 101 (3) (2012).
[124] L. Liu, S. Ryu, M.R. Tomasik, E. Stolyarova, N. Jung, M.S. Hybertsen, M.L. Steigerwald, L.E. Brus, G.W. Flynn, Nano Lett. 8 (7) (2008) 1965–1970.
[125] S. Rumyantsev, G. Liu, W. Stillman, M. Shur, A.A. Balandin, J. Phys.: Condens. Matter 22 (39) (2010) 395302.
[126] Z. Liu, A.A. Bol, W. Haensch, Nano Lett. 11 (2) (2010) 523–528.
[127] M.R. Choudhury, Y. Youngki, J. Guo, K. Mohanram, Nanotechnol. IEEE Trans. 10 (4) (2011) 727–736.
[128] Y. Tianhua, L. Eun-Kyu, B. Briggs, B. Nagabhirava, Y. Bin, Electron Device Lett. IEEE 31 (10) (2010) 1155–1157.
[129] Y. Tianhua, L. Eun-Kyu, B. Briggs, B. Nagabhirava, Y. Bin, Nanotechnol. IEEE Trans. 10 (4) (2011) 710–714.

Dr. Liancheng Wang received his bachelor of science from School of Materials in Central South University of China and his PhD from Institute of Semiconductors, Chinese Academy of Sciences, in 2013. Now he works as a Research Fellow in Luminous! Centre of Excellence for Semiconductor Lighting and Displays, School of Electrical and Electronic Engineering, Nanyang Technological University, Singapore. Dr. Wang's research interests include III-nitride optoelectronic semiconductor material growth, device fabrication and graphene optoelectronics.

Dr Liu Wei is currently working with school of electrical and electronic engineering, Nanyang Technological University, Singapore. He obtained his PhD in electrical engineering from National University of Singapore in 1999. Before he joined Nanyang Technological University he worked in institute of materials research and engineering, Agency of Science, Technology and Research, Singapore. His research interest includes semiconductor epitaxial growth, material characterization and semiconductor device design and fabrication. Currently his research areas include group-III nitride LEDs, GaN power electronics and group-III nitride-based piezotronics and piezo-phototronics.

Mr. Yiyun Zhang received his Masters degree from Institute of Semiconductors, Chinese Academy of Sciences, in 2012. He now has been working for his PhD degree in Department of Electrical and Electronic Engineering at The University of Hong Kong since 2012. His current research interests focus on graphene transparent electrodes and GaN-based semiconductor optical microcavities on Si substrate.

Dr. Zhang Zihui received his bachelor of science from School of Physics in Shandong University of China and PhD in engineering from School of Electronic and Electrical Engineering in Nanyang Technological University of Singapore. Dr. Zhang's research interests include III-nitride optoelectronic semiconductor material including epitaxial growth, material characterization, device fabrication, device physics and device modeling.

Swee Tiam Tan received his B.Eng. and PhD degrees from Nanyang Technological University, Singapore, in 2003 and 2007, respectively. From 2007 to 2010, he was with the Semiconductor Process Technologies Laboratory, Institute of Microelectronics, A*STAR, Singapore. Since 2010, he has been with the Nanyang Technological University, Singapore, where he is currently the Program Manager for LUMINOUS! Centre of Excellence for Semiconductor Lighting and Displays. He has authored or coauthored more than 90 international peer-reviewed journals and two book chapters, and received more than 1600 citations. His current research interests include the epitaxial growth and characterization of III-V and II-VI semiconductor, semiconductor LED lighting, OLED, OPV, and nanocrystal optoelectronics.

Xiaoyan Yi, PhD, Professor, is the deputy director and chief engineer of semiconductor lighting R&D center, Institute of Semiconductors, Chinese Academy of Sciences. Her primary research interest is in the field of nitride materials, devices design, device processing and fabrication, and device characterization. She has made pioneering contributions in the development of Solid-State Lighting in China and participated in several national projects of nitrides field about high-power LED structure design and key technology research. She has received more than $6 million research funding from Ministry of Science and Technology of China, Chinese Academy of Sciences, as well as from the industry. In the recent 3 years, her research has resulted in more than main 46 papers and 50 patents.

Professor Wang Guohong obtained his PhD degree in 1998 and is now working at the Institute of Semiconductors, Chinese Academy of Sciences. He has been a visiting professor in RWTH Aachen University, Nagoya University and Meijo University. He is the member of China Illuminating Engineering Society (CIES). He has been a chair for several National High Technology Programs and National Natural Science Foundations of China. He has authored over 90 peer-reviewed journal publications and has over 80 patents; his research interests focus on group-III nitride LEDs.

Dr. Xiao Wei Sun is presently a full professor of electronic engineering of Nanyang Technological University. He obtained his PhD degree from the Hong Kong University of Science and Technology in 1999. In 2013, he worked in South University of Science and Technology of China as a Chair Professor to set up the Department of Micro/Nano Materials and Devices and then the Department of Electrical and Electronic Engineering. He was awarded the Nanyang Award for Research and Innovation in 2009, the 1000 Talent Award by the Chinese Government in 2012, and the Jacques Beaulieu Excellence Research Chair of INRS (Institut national de la recherche scientifique), Quebec, Canada, in 2013. He is an Academician of the Asia-Pacific Academy of Materials. He is a Fellow of SPIE, a Fellow of Society for Information Display, and a Fellow of the Institute of Physics (UK). He is presently an Adjunct Professor in the Department of Electrical and Electronic Engineering, Hong Kong University of Science and Technology. Professor Sun has authored over 350 peer-reviewed journal publications, and delivered numerous invited talks. According to Web of Science, he has more than 10,000 citations with an h-index of 47.

Dr. Zhu received his B.S. degree in Mechanical Engineering (1998) and PhD degree in Materials Processing Engineering (2003) from Tsinghua University. After Post Doc. researches in Japan and USA, he began his independent career as a faculty member at Tsinghua University (2008-present). He is currently a Professor at the School of Materials Science and Engineering and the State Key Laboratory of New Ceramics and Fine Processing. His current research interests involve macrostructure assembly and engineering of graphene and carbon nanotubes, flexible energy devices (e.g. solar cells, supercapacitors), sensors

and actuators, and membranes for desalination and purification. His expertise includes chemical vapor deposition, solution processing for crystal growth and structure design of nanomaterials.

Professor Hilmi Volkan Demir received his B.Sc. degree in electrical and electronics engineering from Bilkent University, Ankara, Turkey, in 1998, and his M.S. and PhD degrees in electrical engineering from Stanford University, Stanford, CA, in 2000 and 2004, respectively. In 2004, he joined Bilkent University as a faculty member and is an Associate Professor with joint appointments at the Department of Electrical and Electronics Engineering and the Department of Physics. In 2007, he received the Docent title (associate professorship) from the Turkish Council of Higher Education. In 2009, he was awarded the Singapore NRF Fellowship. He is concurrently Nanyang Associate Professor jointly with the School of Electrical and Electronic Engineering and the School of Physical and Mathematical Sciences, Nanyang Technological University, Singapore, and the Director of the LUMINOUS! Center of Excellence for Semiconductor Lighting and Displays. His current research interests include energy-saving LEDs for quality lighting, the science and technology of excitonics for high-efficiency light generation and harvesting and nanocrystal optoelectronics. He has co-authored over 150 SCI journal publications and delivered over 150 invited seminars and lectures in academia and industry. Dr. Demir is the recipient of the European Science Foundation European Young Investigator Award in 2007, the National Scientific Technological Research Council Distinguished Young Scientist Award of Turkey in 2009 and Nanyang Award for Research Excellence in 2013.